Engineering Science and Technology, an International Journal xxx (2016) xxx–xxx

HOSTED BY

ELSEVIER

Contents lists available at ScienceDirect

Engineering Science and Technology, an International Journal

journal homepage: www.elsevier.com/locate/jestch

Full Length Article

Modeling and optimization of process variables of wire-cut electric discharge machining of super alloy Udimet-L605

Somvir Singh Nain [a,*], Dixit Garg [a], Sanjeev Kumar [b]

[a] Department of Mechanical Engineering, National Institute of Technology, Kurukshetra 136119, India
[b] Department of Mechanical Engineering, PEC, University of Technology, Chandigarh 160012, India

ARTICLE INFO

Article history:
Received 2 September 2016
Revised 26 September 2016
Accepted 29 September 2016
Available online xxxx

Keywords:
Support vector machine
Multi-linear regression
Non-linear regression
Grey relational analysis
WEDM
Udimet-L605

ABSTRACT

This paper presents the behavior of Udimet-L605 after wire electric discharge machining and evaluating the WEDM process using sophisticated machine learning approaches. The experimental work is depicted on the basis of Taguchi orthogonal L27 array, considering six input variables and three interactions. Three models such as support vector machine algorithms based on PUK kernel, non-linear regression and multi-linear regression have been proposed to examine the variance between experimental and predicted outcome and preferred the preeminent model based on its evaluation parameters performance and graph analysis. The grey relational analysis is the relevant approach to obtain the best grouping of input variables for maximum material removal rate and minimum surface roughness. Based on statistical analysis, it has been concluded that pulse-on time, interaction between pulse-on time x pulse-off time, spark-gap voltage and wire tension are the momentous variable for surface roughness while the pulse-on time, spark-gap voltage and pulse-off time are the momentous variables for material removal rate. The micro structural and compositional changes on the surface of work material were examined by means of SEM and EDX analysis. The thickness of the white layer and the recast layer formation increases with increases in the pulse-on time duration.

1. Introduction

The Udimet-L 605 has established extensive approval for the aeronautics industries [1]. Hebsur et al. [2] concluded that the Udimet-L605 alloy reveals the preeminent impact resistance on areal weight basis. It has been recognized that Udimet-L605 presents 10% better results in contest with titanium's best alloy IMI 550 and it was known to be more superior than others alloy, mainly at high impact velocities (more than 1100 ft/s). The Udimet-L605 may be perfect for fan containment appliance in supersonic aircraft as a substitute for titanium. This alloy has been utilized in the warm segments of aircraft and land based gas turbine. This alloy could be employed in industrial furnace applications, for instance liner/muffles in higher temperature kilns, bearing races, ball bearings, springs and heart valve, etc. It encompasses the enhanced hot corrosion resistance in a tainted environment of gas turbine due to having enhanced chromium contents.

Wire electric discharge machining is a thermo-electric method of machining. The WEDM is extensively employed in production floor for die making, the cutting/separation of sheet material, prototype manufacturing, aerospace and automotive industries for machining hard materials with intricate shape [3]. The WEDM cutting is epitomized by admirable surface quality (Ra 0.15–2.8) and precision ($\geqslant$0.01 mm) devoid of any internal stress in the work material. It is mandatory for WEDM that the work material should be electrically conductive while the mechanical properties like as toughness, hardness, ductility and brittleness inflict no restriction on its working. WEDM is a unique machining method wherein copper, brass or stratified copper, molybdenum and tungsten wire of dimension 0.05–0.3 mm diameter is employed for cutting the material [4]. As wire never comes in contact with work piece therefore no cutting force is required for machining the work material consequently, the burr-free surface is obtained. For accurate machining, it is essential to keep the wire in tension by make use of the mechanical tension devices. The strong electric current flow through the electrodes consequently, the strong electric field is set-up in the fine gap (0.025–0.05 mm) separating the work material and wire electrode [5]. A series of incessant discrete sparks has been formed amid the work material and wire electrode

* Corresponding author.
E-mail addresses: somveersingh34@ymail.com (S.S. Nain), dixitgarg@yahoo.co.in (D. Garg), skthakkarpec@yahoo.com (S. Kumar).

Peer review under responsibility of Karabuk University.

http://dx.doi.org/10.1016/j.jestch.2016.09.023
2215-0986/

Please cite this article in press as: S.S. Nain et al., Modeling and optimization of process variables of wire-cut electric discharge machining of super alloy Udimet-L605, Eng. Sci. Tech., Int. J. (2016), http://dx.doi.org/10.1016/j.jestch.2016.09.023

Nomenclature

MRR	material removal rate in mm^2/min
SR	surface roughness in (μm)
SVM	support vector machine algorithms
SVR	support vector regression
DOF	degree of freedom
C	constant user define parameters
ε	insensitive loss function
$\|\|w\|\|^2$	Euclidean norm or regularizer defined by Lagrangian
c	decide the offset of the discriminating plane from origin
ξ, ξ'	slack variables
α_i, α_i'	positive Lagrangian multiplier
λ_i, λ_i'	positive Lagrangian multiplier
PUK	Pearson VII universal function
NLR	non-linear regression
pr1, pr2	parameters of the function
MLR	multi-linear regression
NASA	national aeronautics space agency
M6C	tungsten rich carbide precipitates
M23C6	chromium rich carbide precipitates
GRA	grey-relational analysis

due to the potential difference. Consequently, the huge amount of thermal energy has been generated which melt and evaporate the work material. Hence, the bubble formation was taken place on the surface of the work material. When the turn off period is started, then the current was interrupted. Therefore, the abrupt fall in temperature implodes the bubbles causing dynamic force to active on work material. This dynamic force was the reason for projecting the molten material out from the surface of the work material and forms the cavity on the surface of the work material.

In recent years, researchers have made various efforts to evaluate the performance of WEDM on different materials using different modeling and optimization technique. Williams and Rajurker [4] investigated the surface characteristics of WEDM generated surface by using stochastic modeling and analysis technique. SEM and EDX machine were used to better understand the quality of surface. Lee and Li [6] examined the surface characteristics of EDMed tungsten carbide and observed that amount of concentration of WC decreased from the inside surface of the work material to the outer surface of the work material. The percentage of cracks formation on machined surface was increased with increase in pulse-on time and peak current value. Newton et al. [7] investigated the effect of process variables on the recast layer formation on the WEDMed surface of Inconel-718. Antar et al. [8] investigated the behavior of superalloy Udimet-720 and Ti-6Al-2Sn-4Zr-6Mo using coated and uncoated brass wire in WEDM. Kumar and Batra [9] investigated the effect of tungsten powder mixed with dielectric fluid during the electric discharge machining process. Rajyalakshmi and Ramaiah [10] recommended the use of grey relational theory to improve the MRR, SR and spark gap characteristics of WEDM of Inconel-825. Goswami and Kumar [11] utilized the GRA for optimization of process variables in WEDM of Nimonic-80A. Sivaprakasam et al. [12] employed the desirability approach and genetic algorithm for improving the performance characteristics like as MRR, kerf width and SR of WEDM and observed that the voltage (A), feed rate (C), interaction of voltage and capacitance (AB) and pure quadratic effect have a momentous effect on performance characteristics of WEDM. Rajyalakshmi and Ramaiah [13] employed the fuzzy-grey relational approach coupled with Taguchi approach for obtaining the optimal combination of process variables of WEDM. Prasad et al. [14] examined the effect of process parameters of WEDM on damping behavior of A356.2 aluminum alloy. Bobbili et al. [15] investigated the MRR and SR of WEDM of Al 7017 and RHA steel and proposed the Buckingham pi theorem for modeling the WEDM process. The SEM is used for describing the MRR and SR properties of WEDM. Soundararajan et al. [16] examined the effect of pulse-on time, pulse-off time and peak current on MRR and SR of WEDM of A413 alloy by using desirability approach. Unune and Mali [17] worked on low frequency vibration assistant micro-WEDM machine and investigate about the MRR and kerf width of the machine. Nayak and Mahapatra [18] proposed an ANN model for investigating the interplay amid the process variables of WEDM and utilized the bar algorithms for optimization of process variables to reduce the angular error. Some researchers utilized the support vector machine algorithm for modeling the process parameters in WEDM or in statics and civil engineering fields [19–22] etc. Consequently, hardly any work has been reported on the machinability evaluation of Udimet-L605 in WEDM and modeling the process using different machine learning approaches like as SVM, NLR and MLR and optimization of the responses using GRA approach.

Because of unique importance of Udimet-L605 over the IMI 550 alloy (best titanium alloy) and its extensive use in aerospace industries, it was necessary to expose the machinability behavior of Udimet-L605 during wire electric discharge machining. Keeping in view the better performance current study investigates the change in surface characteristics and material removal rate of Udimet-L605 during WEDM and examines the potential of machine learning approaches like as support vector machine algorithms, non-linear and multi-linear regression. The attempts have been done to get the best combination of process variables of WEDM using grey relational analysis and getting the desirable outcome for SR and MRR. In addition to this, the influence of input parameters has been observed in the formation of the white layer, recast layer and compositional change upon the surface during machining in WEDM. In this context, the SEM and EDX have been used to sense the change in surface quality and composition of work material after machining of Udimet-L605 in WEDM.

2. Material and method

This part is consisting of three segments. In the first segment, the detail about the specification and properties of Udimet-L605 used for WEDM will be discussed. In the second segment, the details about experimental set-up and plan will be discussed. In the third segment, details about the procedure of entire three models will be provided for modeling the WEDM process.

2.1. Material

In this research, a plate of the rectangular shape of Udimet-L605 is taken as work material for wire electric discharge machining. Because of its extensive use, Udimet-L605 is called unusually well characterized material. In this context, the machining of Udimet-L605 alloy will be the matter of a lot of examinations to identify its traits over extensive range conditions. The specification of the plate was 400 mm × 150 mm × 6 mm respectively. The total number of 81 square pieces of dimension 12 mm × 12 mm were incises the rectangular plate of Udimet-L605 using WEDM. The chemical

Please cite this article in press as: S.S. Nain et al., Modeling and optimization of process variables of wire-cut electric discharge machining of super alloy Udimet-L605, Eng. Sci. Tech., Int. J. (2016), http://dx.doi.org/10.1016/j.jestch.2016.09.023

composition and mechanical properties of Udimet-L605 has been revealed by Tables 1 and 2.

2.2. Experimental method and design

The experiments were accomplished on the Electronica sprintcut (Electra-Elplus 40A DLX) CNC wire-electric discharge machining as revealed in Fig. 1 and Fig. 2 respectively. Plane brass wire of diameter 0.25 mm has been employed in experimentation on WEDM. Deionized water has been used as a dielectric medium at constant room temperature of 25 °C.

The material removal rate (MRR) is anticipated by means of this formula as follows:

$$MRR = C_s \times t \ (mm^2/min) \quad (1)$$

where the C_s is expressed in mm/min and known as cutting speed while t is expressed in mm and known as thickness of workpiece. The surface roughness of each experiment (SR) were measured using an Accretech surfcom surface contact profilometer with 10 mm evaluation length, speed as 0.3 mm/s and 0.8 mm cutoff value as shown in Fig. 3. The roughness of each piece were examined on three sides of the machined surfaces and three measurements were taken per surface. Therefore, an average of 9 reading/sample was taken as the common roughness of each piece.

Six input parameters specifically known as, pulse-on time duration (Ton), peak current (IP), pulse-off time duration (Toff), wire-feed rate (WF), wire-tension and spark gap voltage (SV) and three interactions such as Ton × Toff, Ton × IP and Toff × IP were designated for the assessment of the performance characteristics of wire electric discharge machining using Udimet-L605 as work material. The entire variables and three interactions were preferred based on pilot experimentation and preceding research. Three levels for every input variable were considered to carry out the experiments as specified in Table 3. The range of these input variables was decided based on pilot experimentation, considering five levels of each parameter by means of one factor at a time approach (OFAT).

Experimental work was intended on the basis of Taguchi method of design of experimentation by means of a L27 orthogonal array. Each input variable is considered to encompass of two degree of freedom. Consequently, the overall DOF linked with input variable and interactions is 24 (6.2 + 3.4). Therefore, L27 orthogonal array is preferred to demonstrate the experimental plan. Based upon the premeditated experimental design as specified in Table 4, total 27 experiments have been performed randomly and each experiment has been repeated three times individually to regard as the experimental error. So total of 81experiments were accomplished in WEDM using Udimet-L605 as work material.

Table 2
Mechanical and physical properties of Udimet-L605.

Properties	Value	Unit
Density	9.27	(g/cm^3)
Melting range	1330–1410	(°C)
Specific heat (at 21 °C)	385	(J/kg°C)
Tensile strength ultimate	862	(MPa)
Tensile strength, yield	310	(MPa)
Elongation	30	(%)
Hardness	277	(Mpa)
Coeff. of expansion (20–93 °C)	12.3	(μm/m°C)
Thermal conductivity	9.4	(W/m°C)
Electrical resistivity (at 24 °C)	0.886	(μΩm)

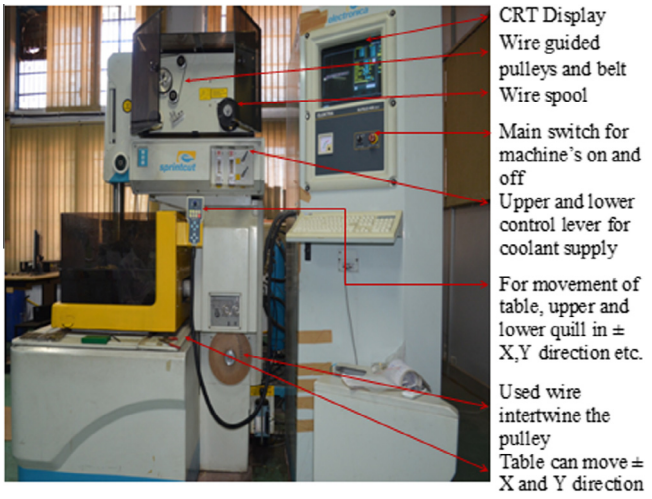

Fig. 1. Experimental setup of WEDM machine.

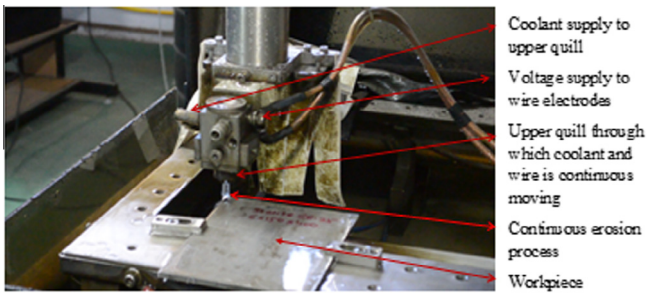

Fig. 2. View of erosion process.

3. Modeling of wire electric discharge machining process

Support vector machine, non-linear and multi-linear based regression mathematical models were developed for the better prediction of MRR and SR characteristics of the wire EDM process on Udimet-L605. Then, identified the co-relation between input and output parameters and best model is selected based on evaluation parameters performance of the model and graph analysis. Experimental work has been performed on WEDM machine considering six inputs or explanatory variables by means of Taguchi orthogonal L27 array and each experiment repeated three times separately as discussed above. Out of 81 observations, data is divided into two sets as one is trained set of 66% observations and other is testing set of 33% observations. Using a training data set, different regression models have been developed using different methodology such as SVM using PUK kernel, non-linear and multi-linear regression. Then adequacy of developed models will be checked on testing data set. The characteristic of training and testing experimental data set were specified in Table 5.

Table 1
Details about the elements comprises by Udimet-L605.

Composition	Cobalt	Chromium	Tungsten	Nickel	Iron	Manganese	Copper
Value Wt. (%)	53.2	19.0	14.4	8.44	3.20	1.20	0.46

Please cite this article in press as: S.S. Nain et al., Modeling and optimization of process variables of wire-cut electric discharge machining of super alloy Udimet-L605, Eng. Sci. Tech., Int. J. (2016), http://dx.doi.org/10.1016/j.jestch.2016.09.023

Fig. 3. Surface roughness tester.

Table 3
Five level input variable table.

Parameters	Level			
	I	II	III	Unit
Pulse-on time (Ton)	106	114	122	Machine unit
Pulse-off time (Toff)	28	38	48	Machine unit
Peak current (IP)	130	160	190	Ampere
Spark-gap voltage (SV)	36	58	80	Volt
Wire tension (WT)	1020	1260	1500	Gm
Wire feed (WF)	6	8	10	m/min

3.1. Support vector machine algorithms

The WEKA 3.7.4 version data mining software is used for support vector machine modeling of WEDM process. It is the collection of numbers of machine learning algorithm, one of them is the support vector machine learning algorithm. It is the classification and regression algorithms, resulting from the theory of statically learning [23]. Support vector machine performs structural risk minimization. The SVM is utilized to generate the classifier with the concept of the linear hyper plane. The selected plane which leaves the largest perimeter amid two classes is called as hyperplane where the perimeter is known as the summation of the space amid hyperplane and nearest points of two classes [24]. SVM can convert the original input space into high dimensional characteristics spaces.

The ε-support vector regression has been proposed by Vapnik [24] by means of commencing a substitute as ε-insensitive loss function and permits that the notion of perimeter could be applied to regression issues. The intention of support vector regression is to recognize the function which covering the ε-deviation commencing to the actual target vectors in the entire training set and it must be existed smooth as possible [25]. Therefore, the training set of p number of samples could be indicated by $\{x_i y_i\}$, where i = 1,. . .p, x_i is symbolized as input vector and y_i is symbolized as the target value. The linear function is expressed as:

$$F(x) = \langle w, x \rangle + c \quad (2)$$

Table 4
Experimental layout and observation data table for MRR and SR.

Exp No.	1 A	2 B	3 A × B	4 A × B	5 C	6 A × C	7 A × C	8 B × C	9 D	10 E	11 B × C	12 F	Run(1) MRR	Run(2) MRR	Run(3) MRR	Mean MRR (mm^2/min)	Run (1) SR	Run (2) SR	Run (3) SR	Mean SR (μm)
1	1	1	1	1	1	1	1	1	1	1	1	1	12.414	14.454	15.074	13.981	1.925	1.993	2.033	1.984
2	1	1	1	1	2	2	2	2	2	2	2	2	14.829	13.978	13.261	14.023	1.796	1.769	1.893	1.819
3	1	1	1	1	3	3	3	3	3	3	3	3	8.008	06.562	07.056	07.209	1.531	1.605	1.549	1.562
4	1	2	2	2	1	1	1	2	2	2	3	3	11.424	12.720	10.022	11.389	1.800	1.820	1.809	1.810
5	1	2	2	2	2	2	2	3	3	3	1	1	06.647	06.505	07.489	06.881	1.272	1.327	1.337	1.312
6	1	2	2	2	3	3	3	1	1	1	2	2	18.167	18.208	14.895	17.090	2.074	1.993	2.224	2.097
7	1	3	3	3	1	1	1	3	3	3	2	2	04.137	04.042	04.119	04.099	0.908	0.905	0.903	0.905
8	1	3	3	3	2	2	2	1	1	1	3	3	07.932	07.094	06.487	07.171	1.570	1.487	1.565	1.541
9	1	3	3	3	3	3	3	2	2	2	1	1	07.958	07.469	10.073	08.500	1.589	1.487	1.513	1.530
10	2	1	2	3	1	2	3	1	2	3	1	2	17.552	17.618	16.053	17.074	2.294	2.362	2.502	2.386
11	2	1	2	3	2	3	1	2	3	1	2	3	26.167	27.190	24.007	25.788	2.452	2.440	2.445	2.446
12	2	1	2	3	3	1	2	3	1	2	3	1	27.324	25.636	22.905	25.289	2.476	2.527	2.453	2.485
13	2	2	3	1	1	2	3	2	3	1	3	1	28.343	27.979	28.635	28.319	2.459	2.406	2.459	2.441
14	2	2	3	1	2	3	1	3	1	2	1	2	23.588	22.861	19.494	21.981	2.369	2.357	2.360	2.362
15	2	2	3	1	3	1	2	1	2	3	2	3	16.722	14.980	18.109	16.603	2.379	2.395	2.426	2.400
16	2	3	1	2	1	2	3	3	1	2	2	3	13.822	12.594	16.901	14.439	2.372	2.291	2.420	2.361
17	2	3	1	2	2	3	1	1	2	3	3	1	07.918	07.189	07.908	07.672	2.057	2.222	2.066	2.115
18	2	3	1	2	3	1	2	2	3	1	1	2	21.953	22.606	22.982	22.514	2.075	2.193	2.077	2.115
19	3	1	3	2	1	3	2	1	3	2	1	3	27.879	27.997	27.792	27.889	2.478	2.546	2.619	2.548
20	3	1	3	2	2	1	3	2	1	3	2	1	18.917	21.606	20.281	20.268	2.483	2.41	2.479	2.457
21	3	1	3	2	3	2	1	3	2	1	3	2	27.909	27.929	27.859	27.899	2.327	2.244	2.313	2.295
22	3	2	1	3	1	3	2	2	1	3	3	2	20.976	22.894	23.588	22.486	2.221	2.355	2.306	2.294
23	3	2	1	3	2	1	3	3	2	1	1	3	26.356	25.908	25.899	26.055	2.193	2.299	2.214	2.235
24	3	2	1	3	3	2	1	1	3	2	2	1	27.964	28.111	28.209	28.094	2.515	2.478	2.526	2.506
25	3	3	2	1	1	3	2	3	2	1	2	1	27.832	28.163	28.291	28.095	2.682	2.706	2.686	2.691
26	3	3	2	1	2	1	3	1	3	2	3	2	23.331	26.889	27.682	25.967	2.618	2.691	2.661	2.657
27	3	3	2	1	3	2	1	2	1	3	1	3	14.846	13.813	13.042	13.900	2.673	2.69	2.605	2.656

Table 5
Characteristics of training and testing data set employed.

Input parameters	Training data				Testing data			
	Min.	Max.	Mean	St. Dev.	Min.	Max.	Mean	St. dev.
Ton	106	122	114	6.593	106	122	114	4.243
Ip	130	160	145	15.141	190	190	190	0
Toff	28	48	38	8.242	28	48	38	8.321
WT	7	11	9	1.648	7	11	9	1.664
SV	36	80	58	18.132	36	80	58	18.305
WF	6	10	8	1.648	6	10	8	1.664

Please cite this article in press as: S.S. Nain et al., Modeling and optimization of process variables of wire-cut electric discharge machining of super alloy Udimet-L605, Eng. Sci. Tech., Int. J. (2016), http://dx.doi.org/10.1016/j.jestch.2016.09.023

where w ∈ R^N and c ∈ R while the $\langle w, x\rangle$ correspond the dot product in space R^N. The vector w decides the direction of the discriminating plane while b establishes the offset of discriminating plane with respect to the origin as mention in Eq. (2) which could be attained by diminishing the regularizer or Euclidean function $||w||^2$ [24]. Consequently, an optimization problem for regression analysis is expressed by Cortes and Vapnik [26] which is described as:

$$Minimize\ \frac{1}{2}||w||^2$$

$$subject\ to\ \begin{cases} y_i - \langle w, x_i\rangle - b & \leqslant \varepsilon \\ \langle w, x_i\rangle + b - y_i & \leqslant \varepsilon \end{cases} \tag{3}$$

The Eq. (3) depends upon the postulation that there be present a function that make available inaccuracy on the training pair which is less in comparative to ε [26]. The slack parameters ξ, ξ′ could be established to permit some additional error and optimization problems specified in Eq. (3) could be expressed as given under in Eq. (4) and pact with infeasible restrictions [26].

$$Minimize\quad \frac{1}{2}||w||^2 + C\sum_{i=1}^{p}(\xi_i + \xi_i')$$

$$subject\ to\ \begin{cases} y_i - \langle w, x_i\rangle - b & \leqslant \varepsilon + \xi_i \\ \langle w, x_i\rangle + b - y_i & \leqslant \varepsilon + \xi_i' \end{cases} \tag{4}$$

where $\xi_i, \xi_i' \geqslant 0$ for all and i represent for i = 1, 2, 3…, p number of samples.

ξ_i, ξ_i' = 0 if saddle points are within the ε tube. If observation points are "above" the tube, ξ_i is the positive disparity amid the observed value and ε then α_i will be non zero. Similarly α_i' will be non zero if the observed points are below the tube. So observed points cannot appear in both regions of tube concurrently, whichever α_i or α_i' will remain non zero awaiting the points appears within the tube, and in this context, both the constraints will be zero as shown in Fig. 4

The constant C > 0 has been known as user defined variable which decided the barter among the minimization of loss function or flatness and the extent by which the variation in the error come extra than ε could be accepted. The problem defined in Eq. (4) is known as primeval objective function. The first term $||w||^2$ is called regularizer. The lower the value of C means more weight has been given to regularizer. If C is infinity all constraints must be satisfied. Typing zero means are equivalent to setting C to infinity. It has been recognized that in the majority of cases the equation (4) could be simply explained by changing it into the dual space formulation [26] and this has been done by swapping the disparities with Lagrangian multipliers [27]. The $\alpha_i, \alpha_i', \lambda_i, \lambda_i'$ are the positive Lagrangian multiplier where i = 1,…p. The Lagrangian of the equation (4) can be shaped by multiplying the Lagrangian multiplier with constraint equation and deducting the outcome from objective function i.e. $||w||^2$ as described in Eq. (5).

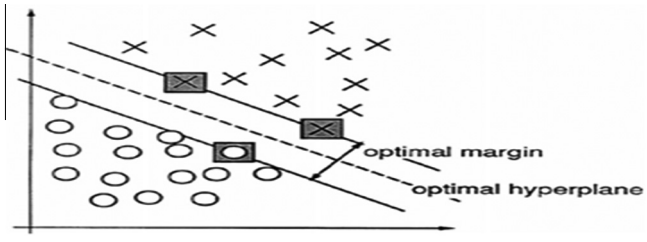

Fig. 4. The support vector, discernible by grey-squares, describes the boundary of the prime division amid two classes [26].

$$L = \frac{1}{2}||w||^2 + C\sum_{i=1}^{p}(\xi_i + \xi_i') - \sum_{i=1}^{p}\alpha_i(\varepsilon + \xi_i - y_i + \langle w, x_i\rangle + b) - \sum_{i=1}^{p}\alpha_i'(\varepsilon + \xi_i' + y_i - \langle w, x_i\rangle - b) - \sum_{i=1}^{p}(\lambda_i\xi_i + \lambda_i'\xi_i') \tag{5}$$

Both the variables in the Eq. (5) have to satisfy the condition as$\alpha_i, \alpha_i', \lambda_i, \lambda_i' \geqslant 0$. The saddle point of a Lagrange function was located to intend the SVM regression of the objective function which could be attained by the derivative of Eq. (5) with respect to b, w, ξ_i and ξ_i' and placing them equivalent to zero forms as follows:

$$\partial_w L = w - \sum_{i=1}^{p}(\alpha_i' - \alpha_i)\cdot x_i = 0 \tag{6}$$

$$\partial_b L = \sum_{i=1}^{p}(\alpha_i' - \alpha_i) = 0 \tag{7}$$

$$\partial_{\xi_i} L = C - \alpha_i - \lambda_i = 0 \tag{8}$$

$$\partial_{\xi_i'} L = C - \lambda_i' - \alpha_i' = 0 \tag{9}$$

By inserting the Eqs. ((6)–(9)) in Eq. (5) results in the configuration of the maximization of an optimization problem is specified as:

$$Maximize\ -\frac{1}{2}\sum_{i=1}^{p}\sum_{j=1}^{p}(\alpha_i' - \alpha_i)\left(\alpha_j' - \alpha_i\right)(x_i \cdot x_j) - \varepsilon\sum_{i=1}^{p}(\alpha_i' + \alpha_i) + \sum_{i=1}^{p} y_i(\alpha_i' - \alpha_i) \tag{10}$$

$$Subject\ to \sum_{i=1}^{p}(\alpha_i' - \alpha_i) = 0\ and\ \alpha_i, \alpha_i' \in [0, C]$$

Dual variables λ_i, λ_i' were removed by using the condition discussed in Eqs. (8) and (9) which can be represented as $\alpha_i' = C - \lambda_i'$ and $\alpha_i = C - \lambda_i$, whereas Eq. (6) can be written as $w = \sum_{i=1}^{p}(\alpha_i' - \alpha_i)\cdot x_i$. The Eq. (10) is a known as a quadratic type problem. Consequently, it may be explained to acquire the values of α_i' and α_i. Now the Eq. (2) could be expressed as:

$$f(x) = \sum_{i=1}^{p}(\alpha_i' - \alpha_i)\langle x_i, x_j\rangle + b \tag{11}$$

The technique explained above could be proficient to permit for non linear support vector regression (SVR) by using the idea of kernel functions [24]. The $x_i \cdot x_j$ in Eq. (10) has been changed with $\Phi(x_i)\cdot\Phi(x_j)$ and optimization problem designed as in Eq. (10) could be expressed as:

$$Maximize\ -\frac{1}{2}\sum_{i=1}^{p}\sum_{j=1}^{p}(\alpha_i' - \alpha_i)\left(\alpha_j' - \alpha_i\right)K(x_i \cdot x_j) - \varepsilon\sum_{i=1}^{p}(\alpha_i' + \alpha_i) + \sum_{i=1}^{p} y_i(\alpha_i' - \alpha_i) \tag{12}$$

$$Subject\ to \sum_{i=1}^{p}(\alpha_i' - \alpha_i) = 0 \text{ and } \alpha_i, \alpha_i' \in [0, C]$$

where K is described as follows:

$$K(x_i, x_j) = \Phi(x_i)\cdot\Phi(x_j)$$

The equations discussed above encourage the use of kernel tricks because no calculation work is required for mapping the $\Phi(x)$ in feature space and computational cost also reduced. Now

the equation (11) could be expressed as shown in equation (14). For the full information about the SVR, reviewers are suggested to follow the Vapnik [24].

$$f(x) = \sum_{i=1}^{p} (\alpha_i' - \alpha_i) K\langle x_i, x_j\rangle + b \tag{13}$$

The selection of kernel function influences the results attained by means of SVR. Therefore, the preference of utilizing the kernel functions is decided after using the different kernel individually. In this context, the Pearson VII universal function (PUK) has been chosen for modeling the WEDM process in the current study. Karl Pearson [28] suggested that the PUK kernel presents good results against the other kernel like as RBF and poly kernel etc. It can be described as follows:

$$K(x_i x_j) = \frac{1}{\left[1 + \left(\frac{2\sqrt{||x_i - x_j||^2}\sqrt{2^{\frac{1}{\omega}}-1}}{\sigma}\right)^2\right]^{\omega}} \tag{14}$$

The variables ω and σ control the tailing factor and the width of the peak. There were some user defined variables like as regularization variable (C), kernel's exact variables and error-insensitive zone ε. The deviation in error-insensitivity zone did not manipulate the envisaged outcomes so the 0.0010 value was taken for the entire running condition [29]. The best value of C, ω and σ were selected after a number of trials with data sets. The value of C, ω and σ were taken one.

3.2. Nonlinear regression

Nonlinear regression is used to model complex phenomena using XLSTAT software. A function is developed and stored in the library of XLSTAT which describes the phenomenon to be modeled and preeminent fit to the model. The fitness of the model is related to the selection of functions. The fitness of the function is determined after a number of trials. The function is defined as follows:

$$Function : pr_1\left(\left(X_1^{pr_2}\right) * \left(X_2^{pr_3}\right) * \left(X_3^{pr_4}\right) * \left(X_4^{pr_5}\right) * \left(X_5^{pr_6}\right) * \left(X_6^{pr_7}\right)\right) \tag{15}$$

pr1, pr2 etc. are the parameters of the function and X1, X2, etc. are the explanatory variables. To assess the relationship between the explanatory and response variables of wire EDM, equation has been developed for MRR and SR using non-linear regression on the training data set as given in Eqs. (16) and (17).

$$MRR = \frac{26.1875\left(Ton^{2.2510} \cdot WT^{0.2807} WF^{1.0102}\right)}{\left(IP^{1.4444} \cdot Toff^{0.5711} \cdot SV^{0.6147}\right)} \tag{16}$$

$$SR = \frac{7.9495 \times 10^{-3}\left(Ton^{2.0906}\right)}{\left(Toff^{0.2514} IP^{0.4617} WT^{0.1089} \cdot SV^{0.2087} \cdot WF^{0.0185}\right)} \tag{17}$$

Then consistency of these equations is examined on the testing data set and analyzes the adequacy of developed regression model.

3.3. Multi-linear regression

Multiple-linear regression is the conversion of the training data set in logarithmic form. The multi-linear regression has been used to form a quantitative reliant parameter Y by means of combining the $X_1 \ldots X_n$ quantitative linear input parameters as shown below.

$$Y = f(X_1, X_2, \ldots X_n) \tag{18}$$

$$\text{Log } Y = f(\text{Log } X_1, \text{Log } X_2, \ldots \text{Log } X_n) \tag{19}$$

where Y is known as dependent parameter and X_1, X_2,...X_n were known as independent variables.

The association amid the Log Y and Log X_1, Log X_2,...Log X_n is recognized using linear regression which is described as follows:

$$\text{Log } Y = \text{Log } a_0 + a_1 \text{ Log } X_1 + a_2 \text{ Log } X_2 \cdots + a_n \text{ Log } X_n \tag{20}$$

After taking the antilog on both sides, the consequent relation is developed as;

$$Y = a_0 X_1^{a_1} \cdot X_2^{a_2} \cdot X_3^{a_3} \ldots\ldots\ldots\ldots X_n^{a_n} \tag{21}$$

The equation generated by multiple-linear regression considered only the parameters which are more effective for a concerned response parameter for which the equation was developed. Equation developed using multiple-linear regression on the training data set will provide the envisaged value of MRR and SR which is described as:

$$MRR = \frac{2.372 \times 10^{-12}\left(Ton^{7.4994}\right)}{\left(Toff^{0.9084} \cdot SV^{0.6748}\right)} \tag{22}$$

$$SR = \frac{1.38963 \times 10^{-6}\left(Ton^{3.5349}\right)}{\left(Toff^{0.3031} WT^{0.244} \cdot SV^{0.224}\right)} \tag{23}$$

Then consistency of these equations was checked on the testing data set to analyze the accuracy of developed regression model. The equations developed by multi-linear regression also give an idea to identify the significant parameters which are more influencing the response variables.

4. Result and discussion

Result and discussion will be complete in four sections. In first segment the performance of entire models will be examined. In the second segment, the single optimization for MRR and SR will be succeeded using Taguchi technique. In addition to this, an investigation concerning the influence of process variables upon the SR and MRR will be made. The third segment demonstrates that the multi-response characteristics will be optimized using grey rational analysis and obtained the optimum value of MRR and SR. In the fourth segment, the microstructure related aspects like as micro crack, crater, white layer and recast layer formation will be discussed.

4.1. Performance evaluation of models for MRR and SR

With the help of support vector machine based on PUK (SVM PUK), nonlinear regression (NLR) and multi-linear regression (MLR), the prophetic value of SR and MRR were detected for each observation in training and testing data set as depicted in Tables 6 and 7. Three parameters like as R^2, R and RMSE were used to examine the outcome of models for the better judgments of the SR and MRR value obtained through the SVM PUK, NLR and MLR methodology. The values of the R^2, R and RMSE for all the models were specified under in Table 8.

Different graphs have been plotted among the experimental and envisaged outcomes for MRR and SR for each model mutually using training and testing data set. To examine the scattering around the perfect line (i.e. Line plotted at an angle of 45 degrees), two other error line in the limit of ±10% has been plotted for the training set and ±20% error line for testing set. The graph among the experimental (actual) values and envisaged value of MRR in WEDM of Udimet-L 605 with training and testing result set is plotted as revealed in the Figs. 5 and 6. Finally, the validation diagram of combined line is plotted between the actual values coupled with

Table 6
Prediction result for MRR and SR obtained by the entire models for training data.

Sr. No.	Ton (μs)	Toff (μs)	IP (A)	WT (g)	SV (V)	WF m/ min	Act. MRR	MRR by NIR	MRR by MLR	MRR by SVM puk.	Act. SR	NLR SR	SR by MLR	SR by SVM. puk
1	106	28	130	7	36	6	12.413	24.309	15.809	14.462	1.925	2.308	2.036	1.997
2	106	28	160	9	58	8	14.829	14.458	11.459	13.997	1.796	1.838	1.721	1.798
3	106	38	130	9	58	10	11.424	16.429	08.683	11.452	1.800	1.865	1.568	1.811
4	106	38	160	11	80	6	6.6471	10.513	06.989	06.691	1.272	1.565	1.390	1.330
5	106	48	130	11	80	8	4.1366	12.454	05.653	04.089	0.908	1.616	1.295	0.904
6	106	48	160	7	36	10	7.9316	13.307	09.689	07.120	1.570	1.814	1.729	1.568
7	114	28	130	9	80	8	17.552	18.865	15.917	17.585	2.294	2.202	2.071	2.359
8	114	28	160	11	36	10	26.167	24.210	27.282	26.152	2.452	2.303	2.358	2.443
9	114	38	130	11	36	6	28.343	27.306	20.673	28.307	2.459	2.370	2.149	2.458
10	114	38	160	7	58	8	23.588	13.331	14.984	22.842	2.369	2.036	2.157	2.359
11	114	48	130	7	58	10	13.822	15.782	12.119	13.833	2.372	2.105	2.009	2.371
12	114	48	160	9	80	6	7.9183	10.243	09.755	07.879	2.057	1.756	1.759	2.064
13	122	28	130	11	58	10	27.879	28.395	32.885	27.845	2.478	2.644	2.693	2.545
14	122	28	160	7	80	6	18.917	15.128	26.470	20.258	2.483	2.382	2.798	2.477
15	122	38	130	7	80	8	20.976	17.202	20.058	22.874	2.221	2.415	2.551	2.303
16	122	38	160	9	36	10	26.356	22.392	34.379	25.931	2.193	2.512	2.869	2.215
17	122	48	130	9	36	6	27.832	26.312	27.805	28.137	2.682	2.632	2.673	2.685
18	122	48	160	11	58	8	23.331	15.429	20.154	26.865	2.618	2.106	2.287	2.659
19	106	28	130	7	36	6	14.454	24.309	15.809	14.462	1.993	2.308	2.036	1.997
20	106	28	160	9	58	8	13.978	14.458	11.459	13.997	1.769	1.838	1.721	1.798
21	106	38	130	9	58	10	12.72	16.429	08.683	11.452	1.820	1.865	1.568	1.811
22	106	38	160	11	80	6	6.505	10.513	06.989	06.691	1.327	1.565	1.390	1.330
23	106	48	130	11	80	8	4.0414	12.454	05.653	04.089	0.905	1.616	1.295	0.904
24	106	48	160	7	36	10	7.0936	13.307	09.689	07.120	1.487	1.814	1.729	1.568
25	114	28	130	9	80	8	17.618	18.865	15.917	17.585	2.362	2.202	2.071	2.359
26	114	28	160	11	36	10	27.190	24.210	27.282	26.152	2.440	2.303	2.358	2.443
27	114	38	130	11	36	6	27.979	27.306	20.673	28.307	2.406	2.370	2.149	2.458
28	114	38	160	7	58	8	22.861	13.331	14.984	22.842	2.357	2.036	2.157	2.359
29	114	48	130	7	58	10	12.594	15.782	12.119	13.833	2.291	2.105	2.009	2.371
30	114	48	160	9	80	6	7.1889	10.243	09.755	07.879	2.222	1.756	1.759	2.064
31	122	28	130	11	58	10	27.997	28.395	32.885	27.845	2.546	2.644	2.693	2.545
32	122	28	160	7	80	6	21.606	15.128	26.470	20.258	2.410	2.382	2.798	2.477
33	122	38	130	7	80	8	22.894	17.202	20.058	22.874	2.355	2.415	2.551	2.303
34	122	38	160	9	36	10	25.908	22.392	34.379	25.931	2.299	2.512	2.869	2.215
35	122	48	130	9	36	6	28.163	26.312	27.805	28.137	2.706	2.632	2.673	2.685
36	122	48	160	11	58	8	26.889	15.429	20.154	26.865	2.691	2.106	2.287	2.659
37	106	28	130	7	36	6	15.074	24.309	15.809	14.462	2.033	2.308	2.036	1.997
38	106	28	160	9	58	8	13.261	14.458	11.459	13.997	1.893	1.838	1.721	1.798
39	106	38	130	9	58	10	10.022	16.429	08.683	11.452	1.809	1.865	1.568	1.811
40	106	38	160	11	80	6	7.4892	10.513	06.989	06.691	1.337	1.565	1.390	1.330
41	106	48	130	11	80	8	4.1193	12.454	05.653	04.089	0.903	1.616	1.295	0.904
42	106	48	160	7	36	10	6.4872	13.307	09.689	07.1201	1.565	1.814	1.729	1.568
43	114	28	130	9	80	8	16.0531	18.865	15.917	17.585	2.502	2.202	2.071	2.359
44	114	28	160	11	36	10	23.9981	24.210	27.282	26.152	2.445	2.303	2.358	2.443
45	114	38	130	11	36	6	28.6347	27.306	20.673	28.307	2.459	2.370	2.149	2.458
46	114	38	160	7	58	8	19.4936	13.331	14.984	22.842	2.360	2.036	2.157	2.359
47	114	48	130	7	58	10	16.9012	15.782	12.119	13.833	2.420	2.105	2.009	2.371
48	114	48	160	9	80	6	7.9077	10.243	09.755	07.879	2.066	1.756	1.759	2.064
49	122	28	130	11	58	10	27.7917	28.395	32.885	27.845	2.619	2.644	2.693	2.545
50	122	28	160	7	80	6	20.2812	15.128	26.470	20.258	2.479	2.382	2.798	2.477
51	122	38	130	7	80	8	23.5882	17.202	20.058	22.874	2.306	2.415	2.551	2.303
52	122	38	160	9	36	10	25.8994	22.392	34.379	25.931	2.214	2.512	2.869	2.215
53	122	48	130	9	36	6	28.2908	26.312	27.805	28.137	2.686	2.632	2.673	2.685
54	122	48	160	11	58	8	27.6818	15.429	20.154	26.865	2.661	2.106	2.287	2.659

the predicted value of MRR and total number of training experiments for the entire models as depicted in Fig. 7. Similarly, the graph between the experimental and the envisaged value of SR in WEDM of Udimet-L 605 is plotted for the training and testing set of entire models as depicted in the Figs. 8 and 9. In the same way, the validation graph has been plotted for SR as revealed by Fig. 10.

4.1.1. Material removal rate evaluation

For the training data of MRR, the value of R, R^2 and RMSE for respective SVM PUK kernel, NLR and MLR models have been depicted in Table 8. Now comparing the performance parameters for each model, it has been concluded that the value of R as well as R^2 was known to be upmost and RMSE value was least for the SVM PUK kernel model in a contest with the entire three models. The Fig. 5 also demonstrated that the most of the predicted values obtained through SVM PUK modeling for the training data set of MRR were existed on perfect line or scattering around it. All the values have been existed between ±10% error lines. While in case of NLR and MLR models, most of the value were deviated from the perfect line or existed out of range of ±10 error lines. Consequently, the SVM PUK model completely dominating the entire models. The testing results as shown in Table 8 and Fig 6 also indicated that SVM PUK kernel model completely dominating the NLR and MLR model and the testing of the model has been conceded. Further, the validation diagram is plotted among the number of training experiments and actual MRR coupled with predicted MRR for the entire models which was depicted in Fig. 7. A dark line indicates the actual MRR line path and dotted lines of different colors indicated the predicted MRR line path for each model. The SVM

Please cite this article in press as: S.S. Nain et al., Modeling and optimization of process variables of wire-cut electric discharge machining of super alloy Udimet-L605, Eng. Sci. Tech., Int. J. (2016), http://dx.doi.org/10.1016/j.jestch.2016.09.023

Table 7
Prediction result for MRR and SR obtained by the entire models for testing data.

Sr. No.	T_{on}	T_{off}	IP	WT	SV	WF	Act. MRR	MRR by NLR.	MRR by MLR	MRR by SVR PUK.	Act. SR	SR by NLR	SR by MLR	SR by SVR PUK
1	106	28	190	11	80	10	08.008	09.816	09.223	17.380	1.531	1.547	1.525	2.067
2	106	38	190	7	36	8	18.167	11.837	11.979	17.145	2.074	1.785	1.856	2.065
3	106	48	190	9	58	6	07.958	08.267	07.023	16.333	1.589	1.490	1.461	2.052
4	114	28	190	7	58	6	27.324	12.346	19.775	17.950	2.476	2.042	2.366	2.133
5	114	38	190	9	80	10	16.722	09.180	12.061	17.782	2.379	1.704	1.888	2.108
6	114	48	190	11	36	8	21.953	13.853	16.720	18.428	2.075	1.865	2.002	2.131
7	122	28	190	9	36	8	27.909	20.752	45.370	19.382	2.327	2.516	3.147	2.167
8	122	38	190	11	58	6	27.964	13.715	24.919	18.530	2.515	2.075	2.455	2.159
9	122	48	190	7	80	10	14.846	08.721	16.223	18.076	2.673	1.903	2.376	2.140
10	106	28	190	11	80	10	06.562	09.816	09.223	17.380	1.605	1.547	1.525	2.067
11	106	38	190	7	36	8	18.208	11.837	11.979	17.145	1.993	1.785	1.856	2.065
12	106	48	190	9	58	6	07.469	08.267	07.023	16.333	1.487	1.490	1.461	2.052
13	114	28	190	7	58	6	25.636	12.346	19.775	17.950	2.527	2.042	2.366	2.133
14	114	38	190	9	80	10	14.980	09.180	12.061	17.782	2.395	1.704	1.887	2.108
15	114	48	190	11	36	8	22.606	13.853	16.720	18.428	2.193	1.865	2.002	2.131
16	122	28	190	9	36	8	27.929	20.752	45.370	19.382	2.244	2.516	3.147	2.167
17	122	38	190	11	58	6	28.111	13.715	24.919	18.530	2.478	2.075	2.455	2.159
18	122	48	190	7	80	10	13.813	08.721	16.223	18.076	2.690	1.903	2.376	2.140
19	106	28	190	11	80	10	07.056	09.816	09.223	17.380	1.549	1.547	1.525	2.067
20	106	38	190	7	36	8	14.895	11.837	11.979	17.145	2.224	1.785	1.856	2.065
21	106	48	190	9	58	6	10.073	08.267	07.023	16.333	1.513	1.490	1.461	2.052
22	114	28	190	7	58	6	22.905	12.346	19.775	17.950	2.453	2.042	2.366	2.133
23	114	38	190	9	80	10	18.109	09.180	12.061	17.782	2.426	1.704	1.888	2.108
24	114	48	190	11	36	8	22.982	13.853	16.720	18.428	2.077	1.865	2.002	2.131
25	122	28	190	9	36	8	27.859	20.752	45.370	19.382	2.313	2.516	3.147	2.167
26	122	38	190	11	58	6	28.209	13.715	24.919	18.530	2.526	2.075	2.455	2.159
27	122	48	190	7	80	10	13.042	08.721	16.223	18.076	2.605	1.903	2.376	2.140

Table 8
Evaluation parameters performance table for MRR and SR.

Model	Training set			Testing set		
	R	R^2	RMSE	R	R^2	RMSE
Material Removal Rate Data set						
SVM PUK kernel	0.9912	0.9817	1.0866	0.7925	0.6280	6.8955
Multiple-linear regression	0.914	0.8355	0.101	0.7692	0.5916	7.0508
Non-linear regression	0.7349	0.54	5.91	0.7736	0.5985	8.3432
Surface Roughness						
SVM PUK kernel	0.995	0.9899	0.252	0.7884	0.6236	0.3593
Multi-linear regression	0.8396	0.705	0.0647	0.62	0.384	0.4299
Non-Linear regression	0.7913	0.626	0.315	0.6996	0.4895	0.3622

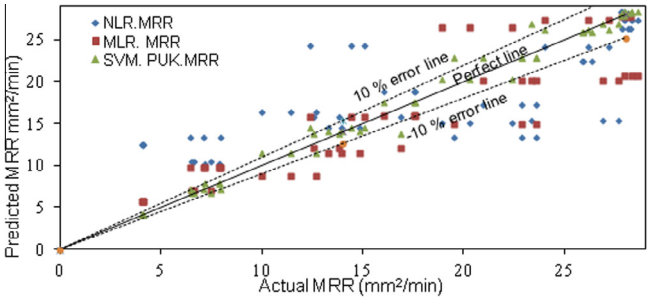

Fig. 5. Graph amide the experimental and envisaged value of MRR (mm^2/min) for training data set.

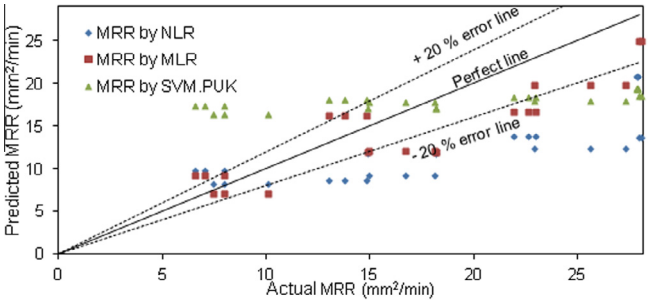

Fig. 6. Graph amide the experimental and envisaged value of MRR (mm^2/min) for testing data set.

based on PUK kernel model line follows the path with close proximity to the actual MRR line in contrast to NLR and MLR model which also prove the dominance of the SVM poly kernel model.

4.1.2. Surface roughness evaluation

Similarly for the training data set of SR, the value of R, R^2 and RMSE for respective SVM PUK kernel model, NLR and MLR models have been depicted in Table 8 which reveals that the value of R as well as R^2 is utmost for SVM poly kernel model in comparison to other models. The RMSE value is least for the SVM PUK kernel model. Consequently the SVM PUK kernel model epitomized the excellent results to prove its dominance over the NLR and MLR models. The testing results also verify the dominancy of the SVM PUK kernel model as revealed in Table 8. Further the Figs. 8 and 9 also revealed that the most of the predicted value for SR were existed on perfect line or scattering around it. All the values have

Please cite this article in press as: S.S. Nain et al., Modeling and optimization of process variables of wire-cut electric discharge machining of super alloy Udimet-L605, Eng. Sci. Tech., Int. J. (2016), http://dx.doi.org/10.1016/j.jestch.2016.09.023

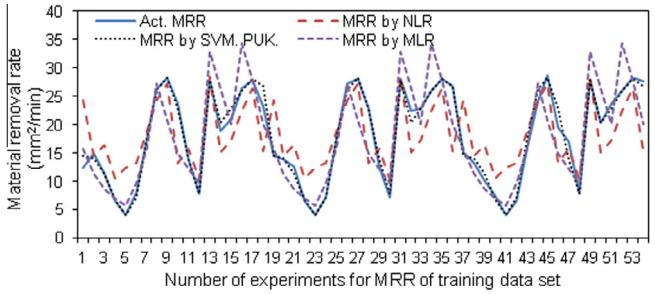

Fig. 7. Validation diagram amid the total number of experiments and actual values of MRR coupled with predicted values of MRR for entire models.

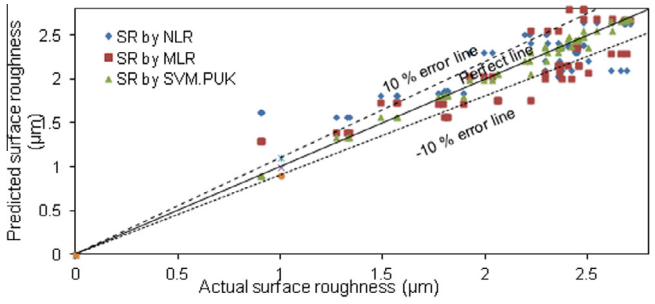

Fig. 8. Graph amid the experimental and envisaged value of SR (μm) for training data set.

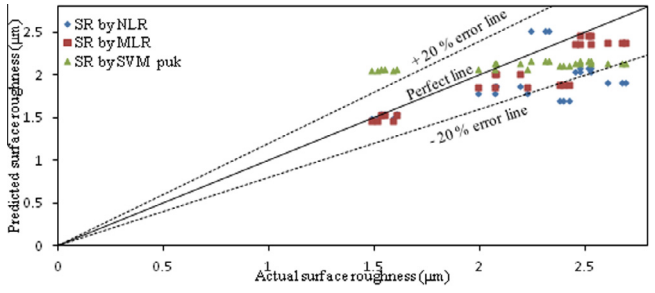

Fig. 9. Graph amid the experimental and envisaged value of SR (μm) for testing data set.

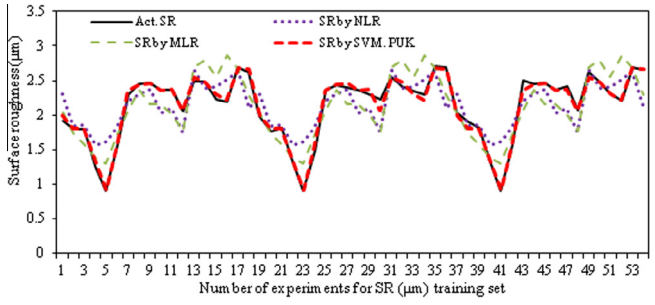

Fig. 10. Validation diagram amid the total number of experiments and actual values of SR coupled with predicted values of SR for entire models.

been existed between ±10% error lines in the training data set and ±20 error line of testing data set. While in case of NLR and MLR models, most of the value have been deviated from the perfect line or existed out of range of ±10 error lines for the training set and ±20 error lines for testing data set. Consequently, the SVM PUK model completely dominating the entire models. Similarly, to MRR the validation diagram has been plotted among the total number of training experiments and actual SR values coupled with predicted SR for all the models which was depicted in Fig. 10. A dark line indicates the actual SR line path and dotted lines of different colors indicate the predicted SR line path for each model. The SVM based on PUK kernel model line follows the path with close proximity to the actual SR line in contrast to NLR and MLR model which also prove the dominance of the SVM poly kernel model.

4.2. Single response optimization for SR and MRR

The Taguchi's technique is used for single response optimization for surface roughness. The Taguchi analysis of experimental data for SR is calculated as follows:

The overall mean of surface roughness (SR) is: $\mu = 2.1485$ μm.

For calculation of confidence intervals, Eq. (24) has been used given by Ross [30].

$$CI_{CE} = \sqrt{F_{\alpha}(1, f_e) \cdot \left\{\frac{1}{n_{eff}} + \frac{1}{R}\right\} \cdot V_e} \tag{24}$$

where

f_e (error degree of freedom) = 2

$F_{0.05}$ (1, 2) = 18.513 (Tabulated value at 95% confidence level)

V_e (error variance) = 0.00074

$n_{eff} = \frac{N}{1+Total\ degrees\ of\ freedom\ involved\ in\ estimation\ of\ mean}$

N = 81, Hence, $n_{eff} = 81/(1 + 12) = 6.231$

R = 3

Putting all the values in the Eq. (24)

$$CI_{CE} = 0.006765$$

The 95% confidence interval for μ_{SR} is $1.0813 < \mu_{SR} < 1.09479$.

The predicted optimum value for SR is calculated as

$$\mu_{SR} == (\mu_{A1} + \mu_{B3} + \mu_{C2} + \mu_{D3} + \mu_{E3} + \mu_{F2}) - 5\mu = 1.0880\ \mu m \tag{25}$$

Fig. 11, Fig. 12 and Table 9 assist the conclusion that all the input parameters and two interactions have significantly influenced the surface roughness of a machined sample of WEDM except the interaction amid the Ton and IP. The SR values were enhanced by the rise in value of Ton, IP and WF and diminished by the rise in SV, WT and Toff as revealed by Fig. 11, the main graph plotted for surface roughness using the MINITAB software. The increase in Ton time duration and at the same instance diminishes in Toff time duration creates high discharge energy which results in melting large amounts of material on the surface of machined sample. Consequently, the big craters have been appearing on the machined surface for high cutting speed as confirmed by SEM image. The poor flushing of molten material due to short duration of Toff time duration results in formation of thick layers of debris and recast layer on surface of machined sample. Consequently, rough surface has been attained as confirmed by SEM image. The surface roughness were diminished with the rise in value of SV due to extending the discharge gap amid the work material and wire electrode. Consequently, less thermal energy has been generated. By the rise in WT, the vibration in wire is reduced, which assist with improvement in surface finishing. All interactions were recognized important at 95% confidence level except the interaction amid Ton and IP (A × C) as revealed by Fig 12 and Table 9.

ANOVA test has been conducted using the MINITAB-16 software in order to examine the significance of input variables on SR. Higher the F value specifies the extent of impact of each input variable for surface roughness of Udimet-L605 at 95% confidence

Please cite this article in press as: S.S. Nain et al., Modeling and optimization of process variables of wire-cut electric discharge machining of super alloy Udimet-L605, Eng. Sci. Tech., Int. J. (2016), http://dx.doi.org/10.1016/j.jestch.2016.09.023

Table 9
ANOVA's outcome for SR.

Source	DF	Seq. SS	Adj SS	Adj MS	F	P	% contribution
A	2	3.88814	3.88814	1.94407	2631.79	0	79.103
B	2	0.11306	0.11306	0.05653	76.53	0.013	2.300
C	2	0.0286	0.0286	0.0143	19.36	0.049	0.5819
D	2	0.16989	0.16989	0.08494	114.99	0.009	3.4561
E	2	0.26302	0.26302	0.13151	178.03	0.006	5.3511
F	2	0.02756	0.02756	0.01378	18.66	0.051	0.5607
A * B	4	0.54409	0.54409	0.13602	184.14	0.005	5.5346
A * C	4	0.04595	0.04595	0.01149	15.55	0.061	0.4675
B * C	4	0.25705	0.25705	0.06426	87	0.011	2.6147
Residual Error	2	0.00148	0.00148	0.00074			0.0003011
Total	26	5.33885					

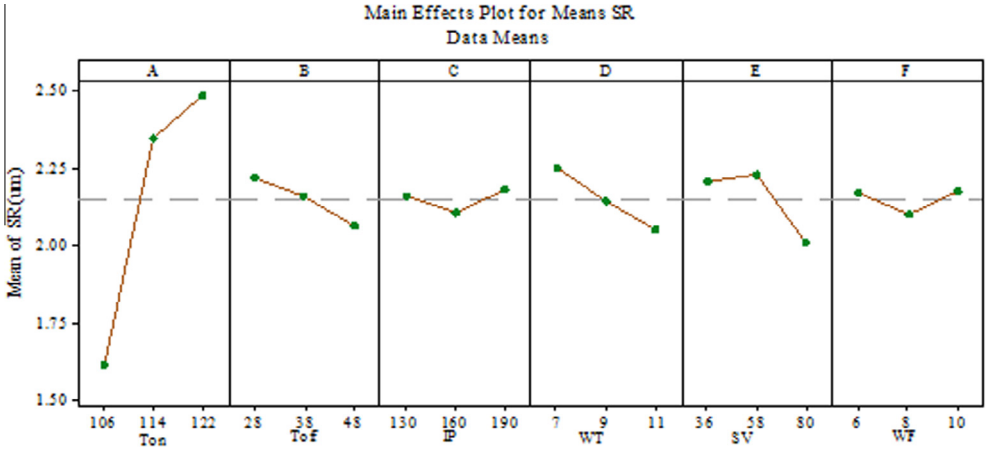

Fig. 11. Main effect plot for the mean value of SR.

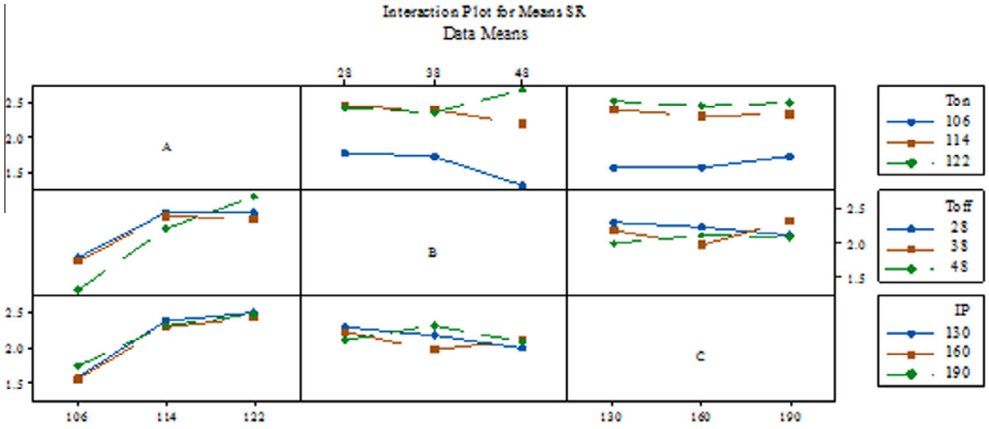

Fig. 12. Interaction plot for mean SR.

level. Similarly, the p value also demonstrates the degree of importance of input variable on concerned response variable. The p value of any significant variables should be less than 0.05 values. Lowest the p value indicates the strong influence of concerned input variables for SR.

The ANOVA results for SR is revealed in Table 9. The Tables 9 demonstrated that all the input variables and interactions under investigation have been known to be significant except the interaction amid Ton and IP (A × C) for the surface roughness. The percentage significance of input variables for SR has been reported as pulse-on time (79.103%), interaction A × B (5.5346%), spark-gap voltage (5.3511%), wire tension (3.4561%), interaction B × C (2.6147%), pulse-off time duration (2.300%), peak current (0.5819%), wire feed (0.5607%) and interaction A × C (0.4675%) respectively. It has been concluded that the Ton, interaction amid Ton and Toff (A × B), SV, WT, interaction amid Toff and IP (B × C) and Toff were the momentous variables for SR against the variables IP, WF and interaction amid the T_{on} and IP.

Similarly, the Taguchi analysis for experimental data set for highest MRR is carried out as follows:

The overall mean of cutting speed: $\mu = 18.1731$ mm^2/min

For calculation of confidence intervals, Eq. (24) is used [30].

$$CI_{CE} = \sqrt{F_{\alpha}(1, f_e) \cdot \left\{\frac{1}{n_{eff}} + \frac{1}{R}\right\} \cdot V_e}$$

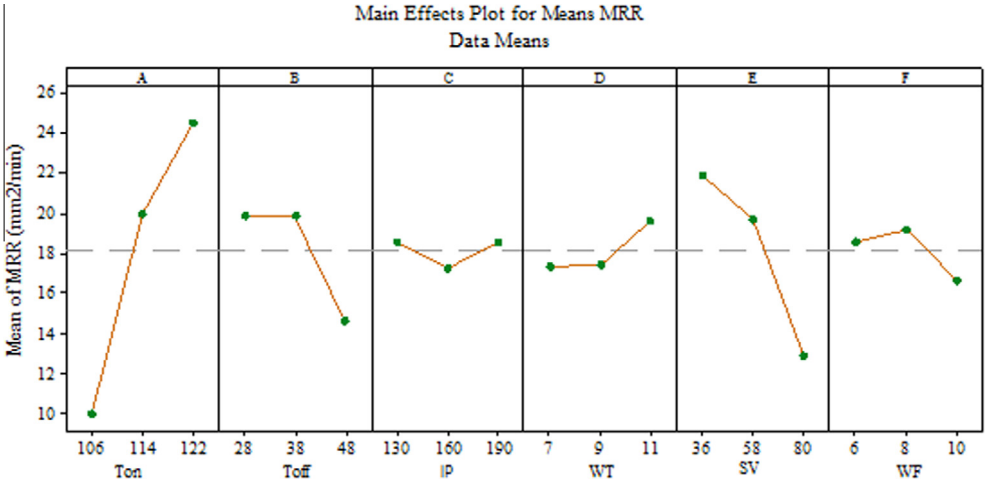

Fig. 13. Main effect plot for mean value of MRR.

Fig. 14. Interaction plot for mean MRR.

$CI_{CE} = 0.9270$

The 95% confidence interval for μ_{CS} is $31.5457 < \mu_{MRR} < 33.3997$. The predicted optimum value for MRR is calculated as

$$\mu_{MRR} = (\mu_{A3} + \mu_{B1} + \mu_{C1} + \mu_{D3} + \mu_{E1} + \mu_{F2}) - 5\mu = 32.4727 \text{ mm}^2/\text{min} \quad (26)$$

Fig. 13 assist the conclusion that the MRR enhanced with a rise in Ton time, wire tension and wire feed rate while diminishing during rising in the value of the SV and Toff time duration significantly. The frequencies of incessant spark generation improved with the rise in Ton time duration. In this context, the rapid melting and vaporization of molten material has taken place which leads to enhance the MRR. With the rise in the value of WF, there will be less probability of dispersing heat to the nearby area. Consequently, high thermal energy has been created in the spark gap, which causes to improve the MRR. In addition to this, the increases in frequency of spark generation lead to more erosion of wire. Consequently, the chances of breaking of wire have been increased. Therefore, it is necessary to supply the wire continuously at optimum speed (8 mm/min) to increase in MRR. Beyond this limit, the increase in the wire feed rate leads to decrease in MRR. The variation in the exact location of wire with respect to the workpiece or vibration in wire decreases with increase in wire tension. Hence the sparks have been concentrating at precise palace and leading to improve in MRR. The decrement of MRR with an increase in SV has been taken place because of extending of average spark gap amid the wire and work material. With the increase in Toff time duration, the occurrence of continuous sparks generation has been decreased. Therefore, decrease in thermal energy generation and it was confirmed by SEM image's Fig. 16. Consequently, the decrease in MRR takes place. The each interaction measured was imperative at 95% of the assurance level statistically as revealed by Fig. 14 and Table 10.

Table 10 demonstrates that all the input variables and interactions under research have been known to be considerable at 95% assurance level of the material removal rate. The percentage significance of input variables on MRR has been reported as pulse-on time (60.1863%), SV (24.0749%), Toff time duration (9.8973%), wire feed (1.8721%), wire tension (1.7736%), interaction A × B (0.7238%), interaction A × C (0.6202%), peak current (0.6126%), interaction B × C (0.2276%), respectively. It has been noted that Ton, SV and Toff are the momentous variables for MRR discern to the variables WF, WT, IP and all interaction.

Table 12 reveals the optimal predicted value and confirmatory experimental value for the single response optimization. The confirmatory experiments were performed three times at the optimal settings of parameters. The mean value of the responses has been found to be within confidence intervals.

4.3. Multi-response optimization

Deng [31] anticipated the grey theory which comprise of grey-relational analysis, grey modeling, prophecy and choice creation of

Table 10
ANOVA table for MRR.

Source	Df	Seq.SS	Adj. SS	Adj. MS	F	P	% contribution
A	2	986.73	986.728	493.364	5257.56	0.000	60.1863
B	2	162.26	162.262	81.131	864.58	0.001	9.8973
C	2	10.04	10.043	5.022	53.51	0.018	0.6126
D	2	29.08	29.078	14.539	154.93	0.006	1.7736
E	2	394.70	394.697	197.349	2103.06	0.000	24.0749
F	2	30.69	30.691	15.346	163.53	0.006	1.8721
A * B	4	23.73	23.734	5.933	63.23	0.016	0.7238
A * C	4	20.34	20.337	5.084	54.18	0.018	0.6202
B * C	4	7.46	7.463	1.866	19.88	0.048	0.2276
Residual error	2	0.19	0.188	0.094			0.0001147
Total	26	1665.22					

a method having incomplete information or the model is unconvinced. It presents a proficient explanation to the ambiguity, large input and distinct problems. This approach is employed to translate the multi-output problems in a single output problem. It presents the relation amid the input and output parameters of the machine. In general, the performance trait of this approach depends upon the calculated grey relational grade. Generally, the grey-relational grade is achieved by taking the average of the grey-relational coefficient (GRC) of MRR and SR. The utmost grey-relational grade was recognized for getting the optimal value of MRR and SR. The optimal level setting of input variables for highest grey-relational grade is accomplished by Taguchi approach.

In grey-relational creation, normalized outcome consequent to lower-the-better condition can be described as:

For SR Lower the Better

$$Y_i^*(k) = \frac{\max x_i^o(k) x_i^o(k)}{\max x_i^o(k) - \min x_i^o(k)} \quad (27)$$

Also, the normalized output consequent to higher-the-better condition can be described as:

For MRR Higher the Better

$$Y_i^*(k) = \frac{X_i^0(k) - \min X_i^o(k)}{\max X_i^o(k) - \min X_i^o(k)} \quad (28)$$

where $Y_i^*(k)$ is the outcome subsequent to the grey relational creation; is the original sequence of mean data before processing where i = 1,2,3,4. . .27. The max $x_i^o(k)$ is selected as the utmost value out of 27 original outcome of $x_i^o(k)$ for the concerned response (kth). Similarly, the min $x_i^o(k)$ is selected as the least value out of 27 original values of $x_i^o(k)$ for the concerned response (kth) where k = 1,2. . .n, and n = 2.

The grey relational coefficient (GRC) is used to characterize the relation amid the desirable and normalized consequences and could be calculated for MRR and SR as follows:

$$£_{ij}(k) = \frac{\Delta_{min} + \zeta\Delta_{max}}{\Delta_{oi}(k) + \zeta\Delta_{max}} \quad (29)$$

where $\Delta_{oi}(k)$ is the divergence of reference sequence which can be articulated as:

$$\Delta_{min} = \min(\Delta_{oi}(k)) = 0 \text{ and } \Delta_{max} = \max(\Delta_{oi}(k)) = 1, \Delta_{oi}(k) = |1 - Y_i^*(k)|,$$

For example GRC can be calculated for MRR and SR for the 1st trial as follow;

$$\Delta_{o1}MRR1 = |1 - Y_i^*(k)| = |1 - 0.408| = 0.592$$

$$\Delta_{o1}SR1 = |1 - Y_i^*(k)| = |1 - 0.3962| = 0.6038$$

By inserting these values in Eq. (29) and calculate for GRC as follows:

$$GRC_{MRR} = (0 + 0.5 \times 1)/(0.592 + 0.5 \times 1) = 0.4579$$

$$GRC_{SR} = (0 + 0.5 \times 1)/(0.6038 + 0.5 \times 1) = 0.4530$$

The ζ is the distinguishing coefficient lies between $0 \leqslant \zeta \leqslant 1$ and its value is set as 0.5 generally [31,32].

The grey-relational grade (GRG) is computed using the following equation:

$$GRG = \frac{1}{n}\sum_{i=1}^{n} w£_{ij}(k) \quad (30)$$

where n represents the performance characteristics, w represent the weight as 0.5 assigned to the each characteristic and $£_{ij}$ (k) is the corresponding GRC for the concerned response traits. The complete analysis of grey rational analysis is depicted in Table 11.

Table 12 demonstrated the confirmation experiment results for the single response optimization using Taguchi's approach and multiple response optimizations using grey relational analysis. Fig. 15 revealed about the main effect graph for the grey relational grade (GRG). Since higher GRG reflects the proximity to the quality characteristics, so it is of 'higher the better' type characteristic. As illustrated in the Fig. 15, the optimum condition of input factor corresponding to maximum GRG is A3B2C1D3E1F1 i.e. Ton time 122 μs, Toff time 38 μs, IP 130 A, WT 11 machine unit or 1500 g, SV 36V and WF 6 m/min. Total three confirmation trials on the optimal setting of variables have been carried out on WEDM and average of them is tabulated in Table 12.

4.4. Microstructure and compositional evaluation of Udimet-L605 after WEDM

After WEDM operations, the scanned electron microscope (SEM) made by Zeiss has been used to investigate the change in surface properties of work material after WEDM process. It has been examined that large number of micro cracks, crater formation, white layer formation and recast layer formation takes place on the surface of the work material after WEDM which were confirmed by SEM image as revealed by Table 13 for different run condition of input variables.

Figs. 16 and 17 shows the change in the micro structural properties of Udimet-L605 for the exp. no. 7th (minimum discharge energy or minimum cutting speed) and exp. no. 13th (high discharge energy) at 1000 × 2000 × and 3000 × magnification level after machining on WEDM. The higher value of pulse-on duration coupled with the lowest value of an SV and Toff time for the experiment 13th (high thermal energy or cutting speed) produced high thermal energy and concentrated in the narrow region between

Table 11
GRA evaluation table for SR and MRR.

Exp. No.	Mean MRR	Mean SR	Mean MRR normalized	Mean SR normalized	Δ MRR	Δ SR	GRC MRR	GRC SR	GRA Grade
1	13.9805	1.9837	0.4080	0.3962	0.5920	0.6038	0.4579	0.4530	0.4555
2	14.0228	1.8192	0.4097	0.4883	0.5903	0.5117	0.4586	0.4942	0.4764
3	7.20880	1.5615	0.1284	0.6326	0.8716	0.3674	0.3645	0.5764	0.4705
4	11.3886	1.8098	0.3010	0.4936	0.6990	0.5064	0.4170	0.4968	0.4539
5	6.88050	1.3120	0.1148	0.7723	0.8852	0.2277	0.3690	0.6871	0.5281
6	17.0898	2.0971	0.5364	0.3327	0.4636	0.6673	0.5189	0.4283	0.4736
7	4.09910	0.9053	00000	1.0000	1.0000	00000	0.3333	1.0000	0.6667
8	07.1708	1.5405	0.1268	0.6444	0.8732	0.3556	0.3641	0.5844	0.4743
9	08.5000	1.5298	0.1817	0.6503	0.8183	0.3497	0.3793	0.5884	0.4839
10	17.0743	2.3861	0.5357	0.1709	0.4643	0.8291	0.5185	0.3762	0.4474
11	25.7881	2.4455	0.8955	0.1376	0.1045	0.8624	0.8271	0.3670	0.5971
12	25.2885	2.4854	0.8752	0.1153	0.1248	0.8847	0.8003	0.3611	0.5807
13	28.3191	2.4413	1.0000	0.1400	00000	0.8600	1.0000	0.3677	0.6839
14	21.9810	2.3619	0.7383	0.1844	0.2617	0.8156	0.6564	0.3801	0.5183
15	16.6034	2.4000	0.5163	0.1631	0.4837	0.8369	0.5083	0.3740	0.4412
16	14.4389	2.3609	0.4269	0.1850	0.5731	0.8150	0.4659	0.3802	0.4231
17	7.67160	2.1148	0.1475	0.3228	0.8525	0.6772	0.3697	0.4247	0.3972
18	22.5136	2.1149	0.7603	0.3227	0.2397	0.6773	0.6760	0.4247	0.5504
19	27.8891	2.5478	0.9823	0.0804	0.0177	0.9196	0.9658	0.3522	0.6590
20	20.2681	2.4573	0.6675	0.1310	0.3325	0.8690	0.6006	0.3652	0.4829
21	27.8988	2.2946	0.9827	0.2221	0.0173	0.7779	0.9666	0.3913	0.6789
22	22.4859	2.2944	0.7592	0.2222	0.2408	0.7778	0.6750	0.3913	0.5332
23	26.0545	2.2352	0.9065	0.2554	0.0935	0.7446	0.8425	0.4017	0.6221
24	28.0944	2.5063	0.9907	0.1036	0.0093	0.8964	0.9817	0.5578	0.7698
25	28.0953	2.6913	0.9908	00000	0.0092	1.0000	0.9819	0.3333	0.6576
26	25.9673	2.6567	0.9029	0.0194	0.0971	0.9806	0.8374	0.3377	0.5876
27	13.9004	2.6560	0.4027	0.0198	0.5953	0.9802	0.4565	0.3378	0.3972

Table 12
Confirmation result table for single and multi-response.

Method	Response	Optimal condition	Optimum predicted value	Confirmatory value
Single response optimization	Material removal rate	A3B1C1D3E1F2	32.4727 mm^2/min	31.5504 mm^2/min
	Surface roughness	A1B3C2D3E3F2	1.08802 μm	1.0057 μm
Grey relational analysis	Material removal rate	A3B2C1D3E1F1		29.3997 mm^2/min
	Surface roughness			2.0917 μm

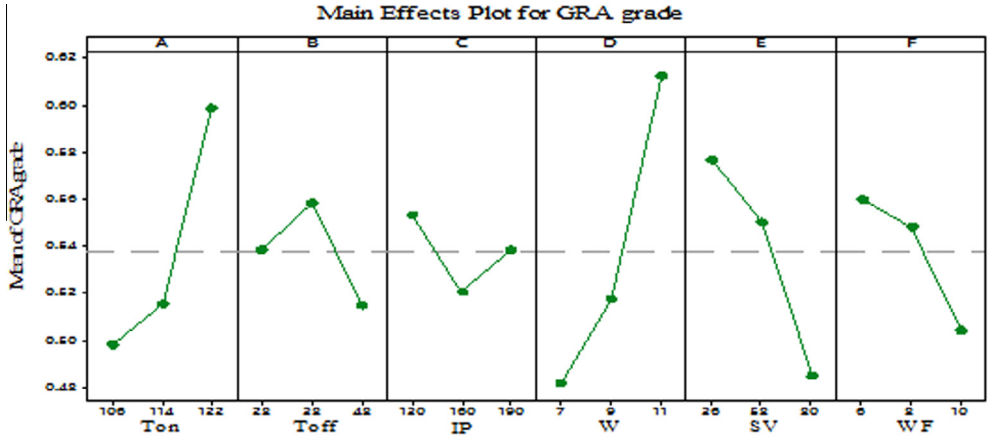

Fig. 15. Main effect plot for mean value of GRA grade.

Table 13
Experiments number under investigation for SEM and EDX analysis.

Experiments	Pulse-on time (T_{on})	Pulse-off time (T_{off})	Peak current (IP)	Wire tension (WT)	Spark gap voltage (SV)	Wire feed (WF)
Experiment no. 7th	106	48	130	1500	80	8
Experiment no.13th	114	38	130	1500	36	6

Please cite this article in press as: S.S. Nain et al., Modeling and optimization of process variables of wire-cut electric discharge machining of super alloy Udimet-L605, Eng. Sci. Tech., Int. J. (2016), http://dx.doi.org/10.1016/j.jestch.2016.09.023

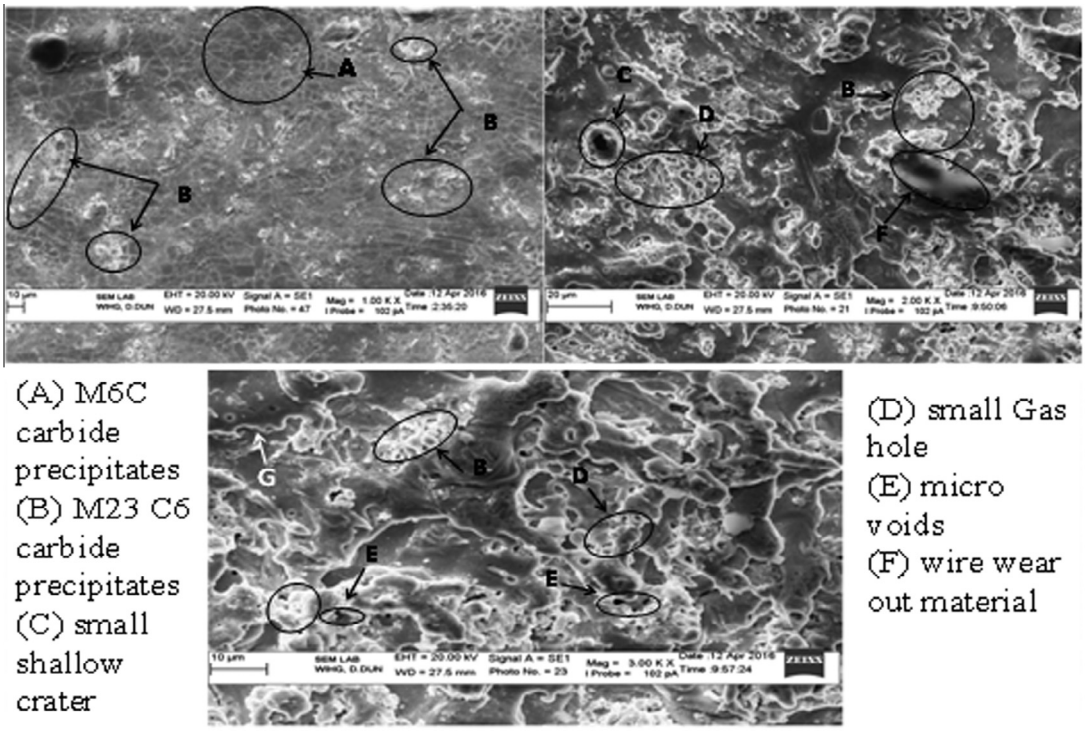

Fig. 16. SEM image for Exp. No 7th (minimum discharge energy) at 1000 × 2000× and 3000 magnification power.

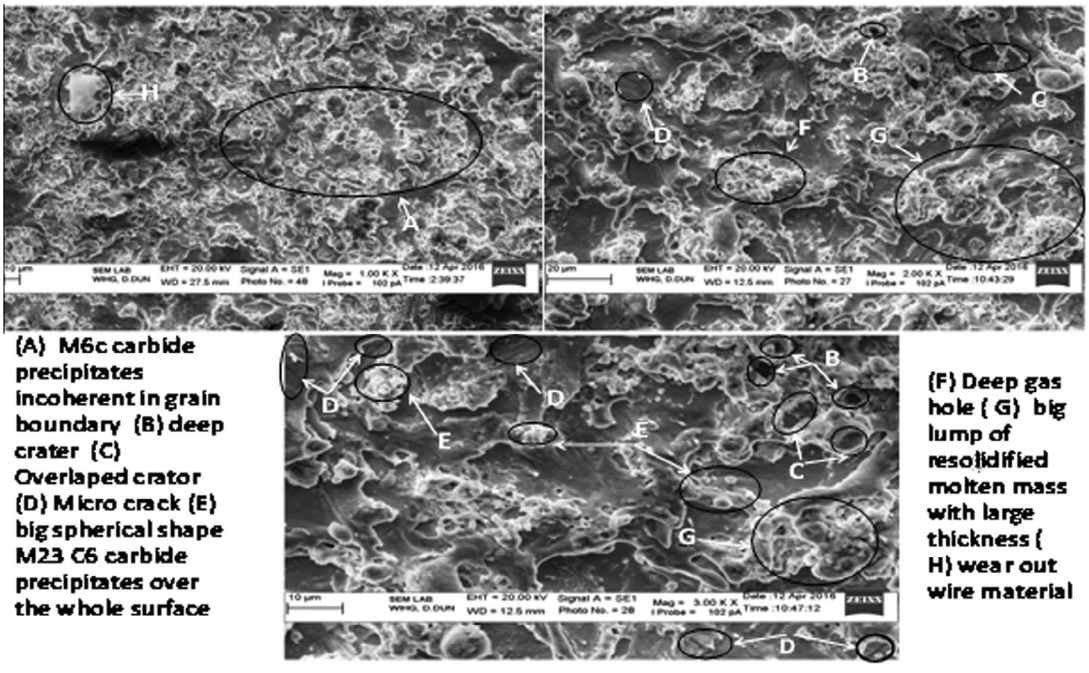

Fig. 17. SEM image of Exp. No. 13th at 1000 × 2000 × 3000 magnification power.

wire and work material. Consequently, big and overlapped craters were observed on the machined surface of material while hardly any craters were observed on the machined surface of the material in the case of the experiment 7th (minimum SR and MRR). The large number of gas holes has been appeared upon the machined surface of materials for both experimental run conditions. The large population of micro cracks has been developed upon the surface of the work material for the running condition of experiment number 13th because the fracture strength of work material is prevailed by high thermal stress created due to the huge amount of thermal energy generation amid the work material and wire [6]. The cracks were formed due to abruptly reduce in thermal energy during pulse-off duration and swiftly supply of dielectric fluid. The cracks were not observed upon the top of machined surface for the

Please cite this article in press as: S.S. Nain et al., Modeling and optimization of process variables of wire-cut electric discharge machining of super alloy Udimet-L605, Eng. Sci. Tech., Int. J. (2016), http://dx.doi.org/10.1016/j.jestch.2016.09.023

running condition of experiment 7th (minimum SR and MRR or minimum thermal energy). Some quantity of molten material among the wire and work material has been flown away with the flow of dielectric fluid and left over molten material re-solidified as recast layer. The large lump of re-solidified molten mass of multiple layers and high thickness has been extended to the whole surface of materials for the running condition of experiment number 13th and the coral reef type surface is obtained. While in case of experiment 7th single layer of re-solidified mass of minimum thickness has been formed and surface obtained was completely smooth. The two types of coarsen precipitates have been also formed on the surface of material incoherent within the grain boundaries and in bulky alloy matrix known as M23C6 and M6C. In the case of exp.7th, very diminutive size primary precipitates M6C (A) with backscattering image formed on the surface of the work material and incoherent within the whole grain boundaries and formed the completely neckless or blocky type structure for the grain of alloy matrix. The M23C6 (B) type precipitates grew in the interior of a grain matrix of alloy and decorated the complete surface with silver or white peaks appearance. While in the case of experiment number 13th, big size and spherical or heart shape M6C and M23C6 carbide precipitates formed and extended to the whole surface of the work material. The spherical shape of precipitates was appeared because of re-solidify molted or vaporized material and it indicated that thermal energy is minimized at the surface of the work material during solidification [33].

4.5. White layer and recast layer analysis after WEDM

The white layer was appearing on top of the machined surface pursued by recast layer. The white layer and recast layer were generally appeared upon the machined surface after WEDM due to re-solidification of molted material. The thickness of the white layer and the recast layer should be minimized in the view of metallurgical point because it leads to develop the micro crack on the machined surface which further leads to fatigue failure of the material and also minimizes the energy dissipation [34,35]. White layer is formed due to the chemical reactivity of oxygen and carbon with the elements of work material and formation of carbide precipitates and oxide takes place on the machined surface in the presence of dielectric fluid. The recast layer is pursued by heat affected zone.

The Fig. 18(A), (B) and (C) shows the SEM image to identify the white layer and the recast layer formed on the surface of the work material for the experiment no. 1st, 7th, and exp. no. 13th. The white layer appeared upon the machined surface for the experiment no. 1st (medium thermal energy or cutting speed) and 13th (high thermal energy or cutting speed) is achieved as 13.41 μm and 15.186 μm respectively. The formation of the white layer on the surface of the work material for the experiment no. 7th (minimum cutting speed and roughness) has been reported as negligible thickness. Consequently, completely smooth surface has been achieved. It was due to the generation of minimum thermal energy amid the wire and work material surface. The thickness of white layer has been identified maximum for the exp no. 13th as 15.186 μm which is due to generation of high thermal energy amid the work material and wire. Consequently, more material has been melted and participated to form the oxides and carbide precipitates of big coarsen size in the presence of dielectric fluid and form the surface as peak and valley type appearance.

Similarly formation of a recast layer depends upon the thermal energy generation and supply of coolant. The thickness of a recast layer for experiment no. 1st, 7th and 13th is identified as 21.57 μm, 9.454 μm and 31.45 μm respectively. The exp. no. 1st was conducted at initial level of all variables consequently; middle range of thermal energy has been created. Therefore, the thickness of recast layer is obtained as 21.57 μm. The thickness of recast layer is lowest as 9.454 μm for exp. No 7th (minimum discharge energy). The highest value of an SV and Toff coupled with the lowest value of Ton and IP for the experiment no. 7th, imparted lowest thermal energy which results in the minimum erosion of material and accessibility to flush out more material due to long pulse-off dura-

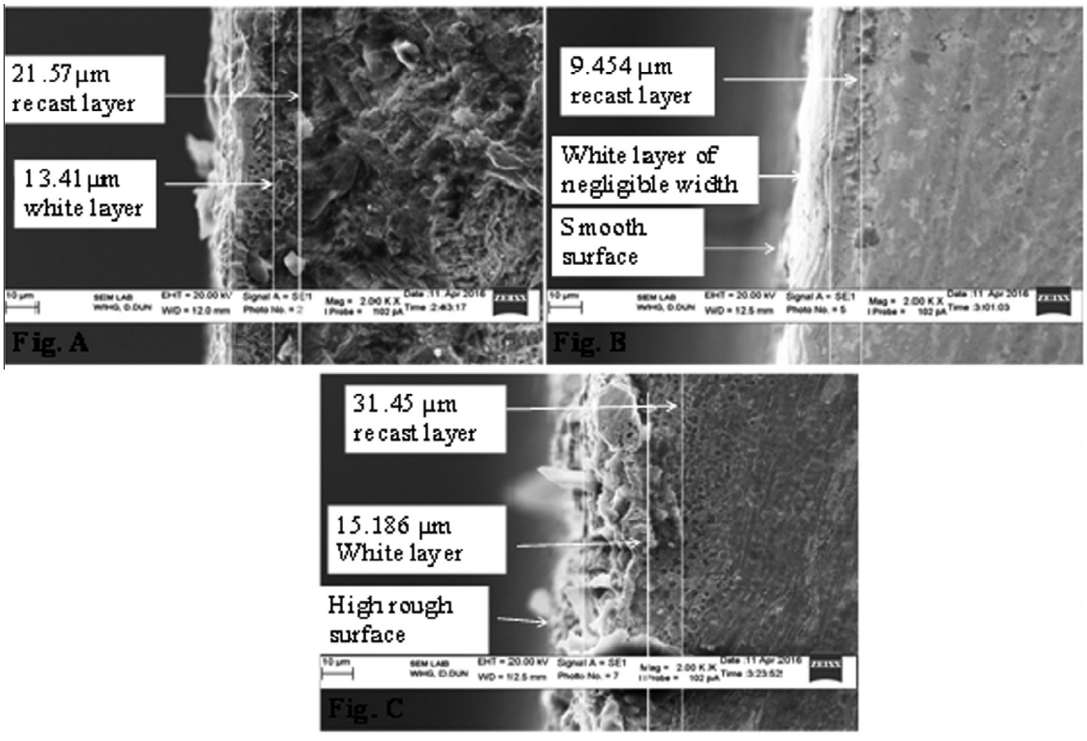

Fig. 18. SEM image analysis of recast layer of the running condition of (a) for exp. number 1st (medium thermal energy) (b) for exp. no. 7th (minimum thermal energy) (c) for exp. number 13th.

Please cite this article in press as: S.S. Nain et al., Modeling and optimization of process variables of wire-cut electric discharge machining of super alloy Udimet-L605, Eng. Sci. Tech., Int. J. (2016), http://dx.doi.org/10.1016/j.jestch.2016.09.023

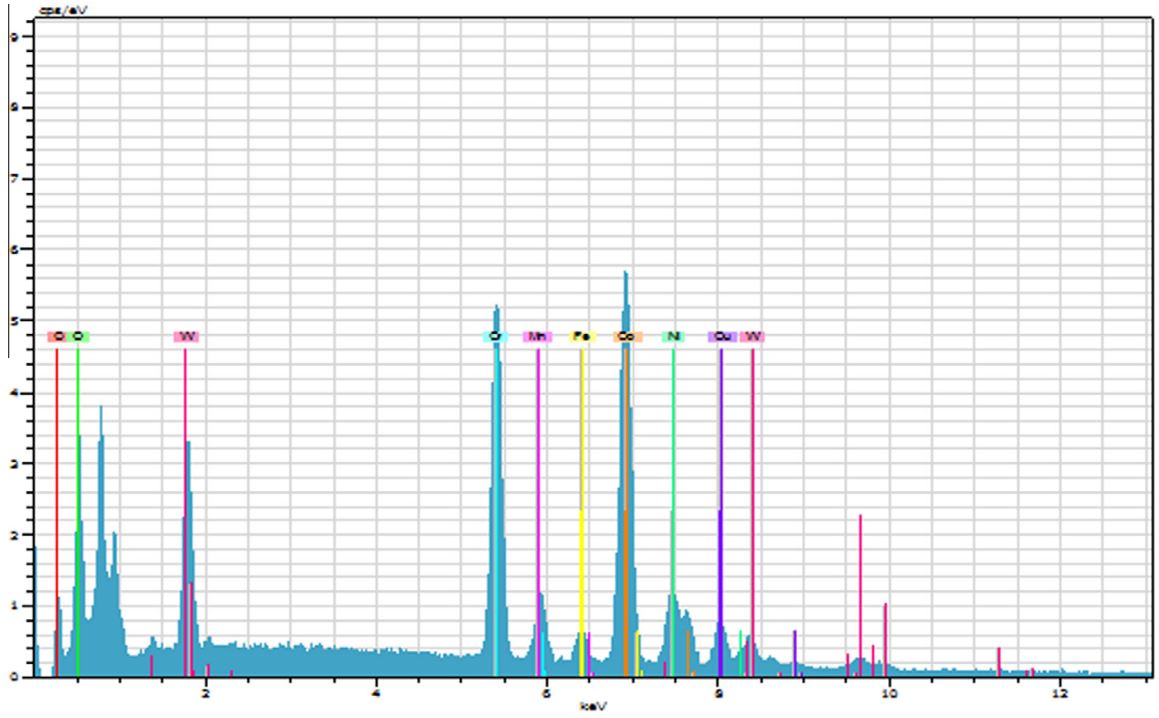

Fig. 19. EDX analysis for experiment no. 7th.

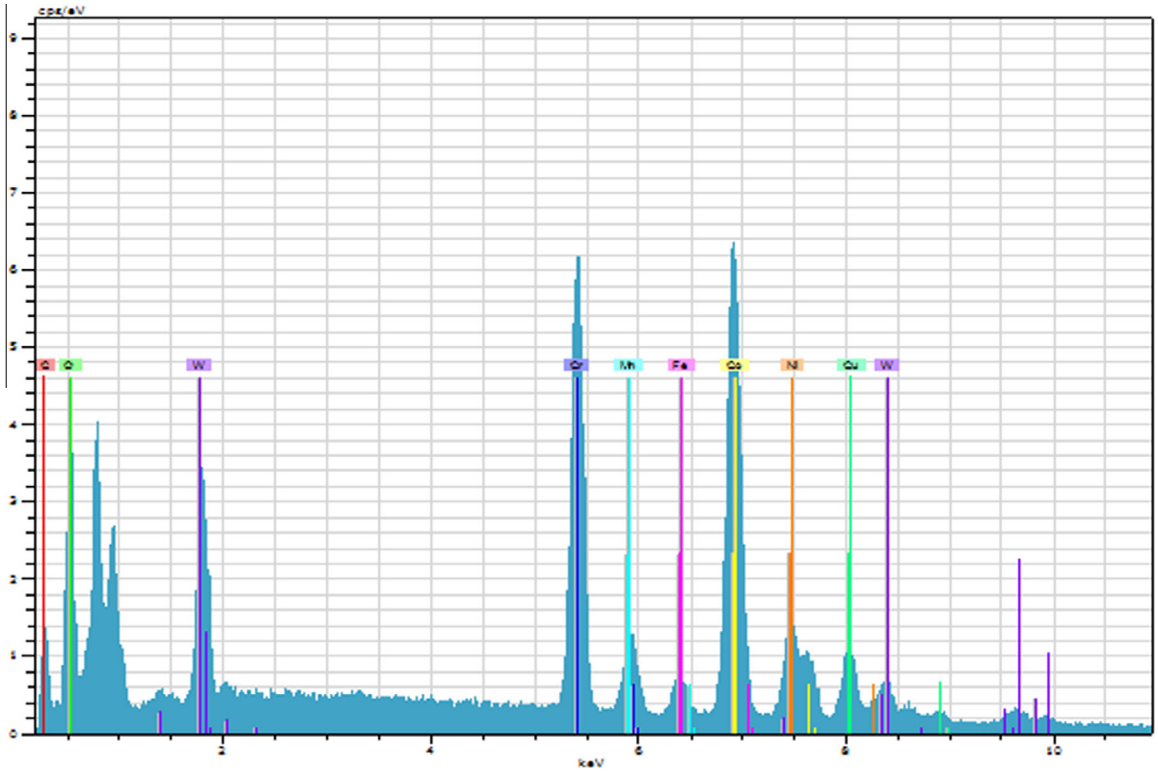

Fig. 20. EDX analysis for exp. no.13th.

tion. Consequently, completely smooth surface has been achieved. The thickness of recast layer is highest for the experiment 13th (maximum cutting speed) due to the large thermal energy generated in the narrow gap between the wire and work material and less accessibility to flush out the molten material. Consequently, the thickness of the recast layer formation has been increased.

4.6. Compositional changes on the machined surface after WEDM

The EDX analysis of experimental no. 7th and experimental no. 13th has been carried out to know the compositional change during WEDM of work material as revealed in Figs. 19 and 20. The Table 14 reveals that the percentage composition proportion of

Please cite this article in press as: S.S. Nain et al., Modeling and optimization of process variables of wire-cut electric discharge machining of super alloy Udimet-L605, Eng. Sci. Tech., Int. J. (2016), http://dx.doi.org/10.1016/j.jestch.2016.09.023

Table 14
EDX compositional result data for the exp. 7th and exp. 13th.

Elements	Before machining (weight %)	Exp. no. 7th (weight %)	Exp. no. 13th (weight %)
Carbon	–	2.52	2.69
Chromium	19	17.76	18.55
Manganese	1.20	1.61	1.86
Iron	3.20	2.08	2.17
Cobalt	53.2	38.37	36.22
Nickel	8.44	8.48	7.77
Copper	0.46	7.05	8.66
Tungsten	14.4	19.21	16.53
Oxygen	–	2.21	3.46

parental elements of Udimet-L605 like as tungsten, nickel, manganese, copper has been increased while cobalt, chromium, iron, decreased for experiment 7th. The presence of carbon and oxygen elements was also noticeable. During thermal erosion process, the tungsten particle leaves the phase of the matrix due to its high atomic weight and come to the surface to participate in carbide precipitate formation. The percentage increase in tungsten elements was more in the experiment 7th against to experiment 13th because of more reactivity of tungsten in comparison to chromium. Another reason may be the reactivity of chromium with carbon and diffusing back to the bulky alloy matrix. The stability of tungsten rich M6C carbide formation were more compare to chromium rich M23C6 carbide precipitates at low thermal energy generated for experiment no. 7th. The size of M6C carbide precipitates was very fine compared to the coarse and big size M23C6 precipitates which resides themselves into the grain boundary of grains and formed blocky type structure. The big size of M23C6 carbide precipitates cannot adjust itself in the grain boundary of grain and may be flushed out more with dielectric fluid. Hence the proportion increases of tungsten was large for exp. no 7th compared to exp. no. 13th. The percentage increase in nickel was very small for exp. no. 7th which may be due to leaving the CO2 laves ($(Co, Ni)_2$(-Cr,W)) phase from the grain boundary phase and act as a driving force to form the M6C carbide precipitates. Hence the percentage of nickel is enhanced on the surface of the material. The percentage of nickel is reduced for the experiment no.13th due to increased stability of chromium affluent secondary precipitates on the surface of the material and nickel may be flushed out with dielectric fluid. The percentage of chromium is diminished on the surface of the material for the experiment no. 7th and experiment no.13th respectively, but the decrease in percentage of chromium is more for experiment no. 7th. This may happen due to the back diffusion of chromium in bulky alloy matrix with reacting carbon at low thermal energy. Another reason may be due to increase in stability of chromium affluent carbide precipitates at high thermal energy generation for experiment 13th. Overall the percentage of chromium was decreased for both running condition because some amount of molten material flushing out regularly with dielectric fluid. The presence of carbon and oxygen content has been found on the surface of the work material after machining on WEDM for both cases, but large in case of experiment no. 13th which may be due to the more swiftly decomposition of dielectric fluid at high thermal energy condition. The brass wire is used in WEDM of Udimet-L605. The large amount of thermal energy has been generated between the wire electrode and work material for the experiment number 13th in contest to experiment number 7th due to which more erosion of wire takes place. Consequently, the percentage increase of copper was large on the surface of the work material for the experiment number 13th against the experiment no. 7th.

5. Unique contribution of research

The key objective of this research was to examine the behavior of Udimet-L605 during WEDM. Both the material and wire-cut electric discharge machining have broad acceptance in aerospace industries. The Udimet-L605 has excellent properties like as creep, tensile strength and impact resistance at high temperature as discussed by different researchers [1,2]. The Udimet-L605 has unique importance over the IMI 550 alloy (best titanium alloy). Therefore, it was necessary to evaluate the machining behavior of material in the presence of high thermal energy. Consequently, WEDM was the best alternative to know the behavior of the material. This research explored the machining characteristics of Udimet-L605 using WEDM which was not discussed before this research has been done. Therefore, this research may be helpful to machinist to know the experimental details of Udimet-L605 during electric discharge machining. An attempt has also been done to observe the significance of different input variables upon the response variables of WEDM using different advanced modeling technique and optimization technique. This research also recommended the use of SVM based poly kernel modeling technique and GRA approach which presents the desirable results.

6. Conclusion

The effort has been done to completely analyze the change in behavior of work material after wire electric discharge machining and it has been concluded that:

1. The support vector machine using PUK kernel presents pre-eminent outcome for surface roughness and material removal rate in contrast to non-linear and multi-linear regression model.
2. The percentage significance of input variables on material removal rate has been reported as pulse-on time (60.1863%), spark-gap voltage (24.0749%), pulse-off time duration (9.8973%), wire feed (1.8721%), wire tension (1.7736%), interaction A x B (0.7238%), interaction A x C (0.6202%), peak current (0.6126%), interaction B x C (0.2276%), respectively.
3. The percentage significance of input variables on the surface roughness has been reported as pulse-on time (79.103%), interaction A x B (5.5346%), spark-gap voltage (5.3511%), wire tension (3.4561%), interaction B x C (2.6147%), pulse-off time duration (2.300%), peak current (0.5819%), wire feed (0.5607%) and interaction A × C (0.4675%) respectively.
4. The pulse-on time have a momentous effect on the material removal rate and surface roughness.
5. Based on grey relational analysis, the best combination of input variable for the desirable outcome of surface roughness and material removal rate is given as: – A3B2C1D3E1F1 or Ton-122, Toff-38, IP-130, WT-11, SV-36 and WF-6 respectively.
6. The micro crack and crater were generally removed in WEDM of Udimet-L605 for the running condition of minimum discharge energy and cutting speed while the large number of crater has been identified for the running condition of highest discharge energy and cutting speed.
7. The thickness of the white layer is negligible at the level of minimum thermal energy and cutting speed. Hence, the completely smooth surface is obtained. The thickness of white layer was highest (15.186 μm) at the level of highest thermal energy and cutting speed.

Please cite this article in press as: S.S. Nain et al., Modeling and optimization of process variables of wire-cut electric discharge machining of super alloy Udimet-L605, Eng. Sci. Tech., Int. J. (2016), http://dx.doi.org/10.1016/j.jestch.2016.09.023

8. The thickness of a recast layer also increased with increase in thermal energy and it was highest (31.45 μm) for the running condition of high discharge energy and lowest for the running condition of minimum thermal energy.
9. The size of M6C precipitates and M23C6 precipitates are very fine in size at minimum cutting speed in comparison to the running condition of the highest speed and appear as white peaks.
10. Based on EDX analysis, it has been concluded that large amount of wire material has been found on the surface of the work material and it was more for the highest cutting speed and less for the lowest cutting speed. The presence of carbon and oxygen are noticeable on the surface of the work material.

Reference

[1] J.S. Wolf, G.D. Sandrock, Some observations concerning the oxidation of the cobalt-base superalloy L-605 (HS-25). NASA TN D-4715 (1968), 1–37. Id. 20020916024.
[2] M.G. Hebsur, R.D. Noebe, D.M. Revilock, Superior ballistic impact resistance achieved by the co-base alloy Haynes 25 (L605), Research and Technology, (2003) NASA/TM-211990.
[3] R. Snoeys, F. Staelens, W. Dekeyser, Current trends in non-conventional material removal processes, CIRP Annal Manuf. Technol. 35 (2) (1986) 467–480.
[4] R.E. Williams, K.P. Rajurkar, Study of wire electrical discharge machined surface characteristics, J. Mater. Process. Technol. 28 (1991) 127–138.
[5] G.F. Benedict, Electrical Discharge Machining (EDM), in: International Conference on Non-traditional Manufacturing Processes, Marcel Dekker, New York & Basel, 1987, pp. 231–232.
[6] S.H. Lee, X. Li, Study of the surface integrity of the machined workpiece in the EDM of tungsten carbide, J. Mater. Process. Technol. 139 (2003) 315–321.
[7] T.R. Newton, S.N. Melkote, T.R. Watkins, R.M. Trejo, L. Reister, Investigation of the effect of process parameters on the formation and characteristics of recast layer in wire-EDM of Inconel 718, Mater. Sci. Eng., A 513 (2009) 208–215.
[8] M.T. Antara, S.L. Soo, D.K. Aspinwall, D. Jones, R. Perez, Productivity and workpiece surface integrity when WEDM aerospace alloys using coated wires, Procedia Eng. 19 (2011) 3–8.
[9] S. Kumar, U. Batra, Surface modification of die steel materials by EDM method using tungsten powder-mixed dielectric, J. Manuf. Processes 14 (1) (2012) 35–40.
[10] G. Rajyalakshmi, P.V. Ramaiah, Multiple process parameter optimization of wire electrical discharge machining on Inconel 825 using Taguchi grey relational analysis, Int. J. Adv. Manuf. Technol. 69 (5–8) (2013) 1249–1262.
[11] A. Goswami, J. Kumar, Investigation of surface integrity, material removal rate and wire wear ratio for WEDM of Nimonic 80A alloy using GRA and Taguchi method, Eng. Sci. Technol. Int. J. 17 (4) (2014) 173–184.
[12] P. Sivaprakasam, P. Hariharan, S. Gowri, Modeling and analysis of micro-WEDM process of titanium alloy (Ti–6Al–4V) using response surface approach, Eng. Sci. Technol. Int. J. 17 (4) (2014) 227–235.
[13] G. Rajyalakshmi, P.V. Ramaiah, Application of Taguchi, fuzzy-grey relational analysis for process parameters optimization of WEDM on Inconel-825, Indian J. Sci. Technol. 8 (35) (2015) 1–12.
[14] D.S. Prasad, C. Shoba, K.R. Varma, A. Khurshid, Influence of wire EDM parameters on the damping behaviour of A356. 2 aluminium alloy, J. Alloy. Compd. 646 (2015) 257–263.
[15] R. Bobbili, V. Madhu, A.K. Gogia, Modelling and analysis of material removal rate and surface roughness in wire-cut EDM of armour materials, Eng. Sci. Technol. Int. J. 18 (4) (2015) 664–668.
[16] R. Soundararajan, A. Ramesh, N. Mohanraj, N. Parthasarathi, An investigation of material removal rate and surface roughness of squeeze casted A413 alloy on WEDM by multi response optimization using RSM, J. Alloy. Compd. 685 (2016) 533–545.
[17] D.R. Unune, H.S. Mali, Experimental investigation on low-frequency vibration assisted micro-WEDM of Inconel 718, Eng. Sci. Technol. Int. J. (2016).
[18] B.B. Nayak, S.S. Mahapatra, Optimization of WEDM process parameters using deep cryo-treated Inconel 718 as work material, Eng. Sci. Technol. Int. J. 19 (1) (2016) 161–170.
[19] L. Zhang, Z. Jia, F. Wang, W. Liu, A hybrid model using supporting vector machine and multi-objective genetic algorithm for processing parameters optimization in micro-EDM, Int. J. Adv. Manuf. Technol. 51 (2010) 575–586.
[20] H. Liu, X. Wang, D. Tan, L. Wang, Study on traffic information fusion algorithm based on support vector machines, in: Proceeding of Sixth International Conference on Intelligent Systems Design and Applications, vol. 6, IEEE, 2006, pp. 183–187.
[21] M. Pal, N.K. Singh, N.K. Tiwari, Support vector regression based modelling of pier scour using field data, Eng, Appl. Artif. Intell. Elsevier 24 (5) (2010) 911–916.
[22] D. Laha, Y. Ren, P.N. Suganthan, Modeling of steelmaking process with effective machine learning techniques, Expert Syst. Appl. 42 (2015) 4687–4696.
[23] V.N. Vapnik, Statistical Learning Theory, John Wiley and Sons, New York, 1998.
[24] V.N. Vapnik, The Nature of Statistical Learning Theory, Springer-Verlag, New York, 1995.
[25] A.J. Smola, Regression estimation with support vector learning machines, Master's Thesis, Technical University, Munchen, Germany, 1996.
[26] C. Cortes, V.N. Vapnik, Support vector networks, Mach. Learn. 20 (3) (1995) 273–297.
[27] D.G. Luenberger, Linear and Nonlinear Programming, 2nd ed., Addison-Wesley, Reading Massachusetts, 1984.
[28] K. Pearson, Contributions to mathematical theory of evolution: II. Skew variation in homogeneous material, Philos. Trans. R. Soc., London, U. K. 186 (A) (1895) 343–414.
[29] I.H. Witten, E. Frank, Data Mining: Practical Machine Learning Tools and Techniques, Morgan Kaufmann, San Francisco, 2005. 2.
[30] P.J. Ross, Taguchi Techniques for Quality Engineering, McGraw Hill, New York, 1996.
[31] J. Deng, Introduction to grey system, J. Grey Syst. 1 (1989) 1–24.
[32] J. Deng, Control problems of grey systems, Syst. Control Lett. 5 (1982) 288–294.
[33] C.A. Huang, F.Y. Hsu, S.J. Yao, Microstructure analysis of the martenstic stainless steel surface fine-cut by the wire electrode discharge machining (WEDM), Mater. Sci. Eng., A 371 (1) (2004) 119–126.
[34] D.S. Prasad, C. Shoba, B.S. Prasad, Effect of white layer on the damping capacity of metal matrix composites, Mater. Sci. Eng., A 591 (2014) 78–81.
[35] D.S. Prasad, C.H. Shoba, Effect of heat treatment on the white layer and its effect on the damping behavior of metal matrix composites, Mater. Sci. Eng., A 599 (2014) 25–27.

Please cite this article in press as: S.S. Nain et al., Modeling and optimization of process variables of wire-cut electric discharge machining of super alloy Udimet-L605, Eng. Sci. Tech., Int. J. (2016), http://dx.doi.org/10.1016/j.jestch.2016.09.023